Late Miocene Unroofing of the Inner Lesser Himalaya Recorded in the NW Himalaya Foreland Basin

Elise M. Exnicios[1], Andrew Carter[2], Yani Najman[3], Peter D. Clift[1,4]

1 - Department of Geology and Geophysics, Louisiana State University, Baton Rouge, LA 70803, USA

2 - Department of Earth and Planetary Sciences, Birkbeck College, University of London, London WC1E 7HX, UK

3 - Lancaster Environment Centre, Lancaster University, Lancaster, LA1 4YQ, UK

4- Research Center for Earth System Science, Yunnan University, Kunming, Yunnan Province, 650091, PR China

ABSTRACT: Testing models that link climate and solid Earth tectonics in mountain belts requires independent erosional, structural and climatic histories. Two well preserved stratigraphic sections of the Himalayan foreland basin are exposed in NW India. The Jawalamukhi (13–5 Ma) and Joginder Nagar sections (21–13 Ma) are dated by magnetostratigraphy and span a period of significant climate change and tectonic evolution. We combine sediment geochemistry, detrital zircon U-Pb dating, and apatite fission track analyses to reconstruct changes in the patterns of erosion and exhumation in this area from the Early Miocene to Pliocene. The provenance of the foreland sediments reflects a mixture of Tethyan and Greater Himalayan sources from 21 to 11 Ma, with influx from the Inner Lesser Himalaya starting after 11 Ma, and a strong increase in Crystalline Inner Lesser Himalayan erosion after 8 Ma. This distinct shift in provenance most likely reflects exhumation of the Kullu-Rampur Window, as well as the northward motion of the Jawalamukhi section towards the Himalayas, drainage reorganization in the foreland, and/or tectonically driven drainage capture in the mountains. Prior to 10.5 Ma sediment came from a large river whose sources were Greater Himalaya and Haimanta dominated, likely a paleo-Sutlej, while after 8 Ma the source river was dominated by a more local drainage. Our work is consistent with Nd isotope and mica Ar-Ar constraints from the same sections that demonstrate initial Inner Lesser Himalayan unroofing in this region from 11 Ma, earlier than the 2 Ma implied from the marine record and during a period of summer monsoon weakening when fission track data indicate very rapid cooling and erosion of the Lesser Himalaya sources from no later than10 Ma. Tectonically driven rock uplift coupled with southerly migration of the maximum rainfall belt during a time of drying, may have focused erosion over the Lesser Himalayan Duplex and created the Kullu-Rampur Window.

Keywords: Provenance, exhumation, Himalayas, monsoon, zircon

1. Introduction

What processes control the structural and topographic development of mountain chains? Tectonic forces cause thickening of continental crust by folding and thrusting, driving uplift of the Earth's surface, while extensional tectonics and erosion allow deep buried rocks to be brought to the surface and topography to be flattened. It is increasingly recognized that the structure of mountain belts reflects the interplay between these two competing forces, although much of our understanding is derived from models rather than observations (Davis *et al.*, 1983; Beaumont *et al.*, 2001; Willett *et al.*, 2003; Robinson *et al.*, 2006). These models suggest that focused erosion, often caused by precipitation or glaciation in a restricted area, can drive asymmetric exhumation and control the pattern of outcrop in compressional orogens. The Himalayas represent a classic example of how climatic development, especially of the South Asian summer monsoon, might interact with the structure and metamorphic history of a mountain chain (Wobus *et al.*, 2003; Thiede *et al.*, 2004; Clift *et al.*, 2008).

Due to overprinting by metamorphism, subduction to great depths, and erosion of bedrock once it reaches the surface, much of the record of an orogen's early history is typically lost from the modern outcrop of the high ranges. Rocks now at the surface can only be used to reconstruct the uplift and cooling of those particular units, but the older history of the Himalayas can only be reconstructed from the erosional record preserved in the foreland basin and/or the deep-sea submarine fans of the Indian Ocean (France-Lanord *et al.*, 1993; Clift *et al.*, 2001; Curray *et al.*, 2003; McNeill *et al.*, 2017).

Here we use new detrital zircon U-Pb dating and apatite fission analysis to explore the links between tectonics, erosion and regional climate using a uniquely well-preserved sediment record from the foreland basin in the NW Himalayas spanning >20 m.y. to test whether changes in erosion patterns and rates are linked to variations in summer monsoon rains, or whether they might instead be tied more closely to tectonic forces. We evaluate reconstructions for provenance evolution derived from earlier work on the same sedimentary section: petrography and detrital mica Ar-Ar dating that proposed a switch in the location of maximum erosion from the Greater Himalaya (GHS) to either Tethyan Himalaya (THS)/Haimanta rocks (Fig. 1) (White *et al.*, 2002) or Outer Lesser Himalayan (OLH) rocks (Colleps *et al.*, 2019) starting at 17 Ma; similar data and bulk mudstone Nd and Sr isotopes were also used to propose an initial unroofing of the unmetamorphosed Inner Lesser Himalaya (ILH) after 11 Ma and the Inner Lesser Himalayan Crystalline Series (LHCS) after 6 Ma (Najman *et al.* (2009) and note correction in Najman *et al.* (2010)). We note that the ILH structurally underlie the OLH so that the two units are sometimes referred to as Lower and Upper LH by some workers, especially further east (Myrow *et al.*, 2015; DeCelles *et al.*, 2016). In doing so we further explore the use of proximal foreland records compared to regional submarine fan records in reconstructing the growth and erosion of orogenic belts. The foreland offers the opportunity for significant sediment sequestration and later reworking and resedimentation to a more distal location, complicating the source-to-sink transport history and thus interpretation of marine sediments deposited at any given time. The proximal records are also more able to sample limited stretches of the mountain front rather than integrating the whole catchment. In doing so, foreland sediment can record along strike changes in erosion and highlight details that are diluted beyond recognition in the deep sea fan.

2. Regional Setting

The Himalayas have formed as a result of continent-continent collision between India and Eurasia, likely starting around ~55–50 Ma in the NW Himalayas (Green *et al.*, 2008; Najman *et al.*, 2017) but potentially as recently as 34 Ma (Aitchison *et al.*, 2007) or even 20–25 Ma for collision between the Indian craton and Eurasia (van Hinsbergen *et al.*, 2012)}. Collision in the NW Himalayas may have slightly postdated collision in the central and eastern parts of the Indus-Yarlung Suture Zone (DeCelles *et al.*, 2014; Wu *et al.*, 2014). The Himalayas consist of a number of east-west striking, thrust-bound tectonic units, described, from south to north, below.

In the Sub-Himalayas of NW India and Pakistan, a Cenozoic marine to continental foreland basin sequence is exposed, which comprises sedimentary rocks shed from the orogen (Parkash *et al.*, 1980; Johnson *et al.*, 1985; Badgley & Tauxe, 1990; Sorkhabi & Arita, 1997; Ravikant *et al.*, 2011). These foreland sediments represent an invaluable archive of the early development of the mountain belt (Meigs *et al.*, 1995; Burbank *et al.*, 1996; Najman, 2006) spanning important climatic and environmental transitions, especially around 7–8 Ma when the climate dried, oceanic upwelling increased and vegetation in the foreland shifted from being C3 to C4 dominated (Quade *et al.*, 1989; Kroon *et al.*, 1991; Clift *et al.*, 2020; Zhou *et al.*, 2021), as well as more recently identified older changes in wind and oceanography in the Arabian Sea starting around 11–13 Ma (Gupta *et al.*, 2015; Bialik *et al.*, 2020).

The Sub-Himalayas represent the most southerly range within the orogen (Figs. 1 and 2), The Neogene Siwalik Group to the south are separated from the older Dharamsala Group to the north by the Palampur Thrust (Thakur *et al.*, 2010). In turn these are separated from the overriding Lesser Himalayas (LH) by the Main Boundary Thrust (MBT), while they now overthrust undeformed floodplains to the south along the Main Frontal Thrust (MFT). The LH can be divided into two units, the Outer and Inner (Robinson *et al.*, 2001; Myrow *et al.*, 2015). The OLH comprise Neoproterozoic to Cambrian sedimentary rocks believed to have been deposited on the Indian passive margin synchronously with the sediments now forming the GHS (Célérier *et al.*, 2009; McKenzie *et al.*, 2011; Hughes, 2016). In contrast, the ILH range from Meso- and Paleoproterozoic sedimentary rocks (Tewari, 2003; McKenzie *et al.*, 2011) to ~1.85 Ga schists and gneisses of the LHCS (Miller *et al.*, 2000; Richards *et al.*, 2005).

The LHs are overthrust by the high-grade metamorphic rocks and leucogranites of the GHS along the Main Central Thrust (MCT). The extensional South Tibet Detachment (STD) separates the Tethyan Himalayan Series (THS), which and its higher-grade basal unit, the Haimanta Group, from the underlying GHS (Frank *et al.*, 1995; Thakur & Tripathi, 2008). All of these units represent rocks that were originally part of the Indian northern passive margin prior to collision, with the GHS representing the result of the Cenozoic metamorphism associated with the orogeny. The THS is back-thrusted towards the north on the Great Counter Thrust that places THS meta-sedimentary rocks on top of the sequences of the Indus Suture Zone (Murphy & Yin, 2003; Yin, 2006), as well as the forearc to Eurasia, represented by the Indus Group in the NW Himalaya (Brookfield & Andrews-Speed, 1984; Garzanti *et al.*, 1987; Henderson *et al.*, 2010).

The sedimentary section we study encompasses the time of exhumation of the LH, and we therefore provide more detail on the evolution of this unit:

The LHs comprise an accretionary duplex whose origin may date back to ~20 Ma (Bollinger *et al.*, 2004). The Tons Thrust that separates the ILH from the OLH is believed to have been active by 16 Ma, with OLH exhumation after this time (Myrow *et al.*, 2015; Colleps *et al.*, 2019). Formation of a mid-crustal structural ramp at 11–12 Ma drove the duplexing of the ILH (DeCelles *et al.*, 1998b), now exposed in the Kullu-Rampur Window (Colleps *et al.*, 2019), from ~11 Ma (Thiede *et al.*, 2004; Vannay *et al.*, 2004; Caddick *et al.*, 2007) before the Pliocene LH duplexing favored by Robinson *et al.* (2006) in western Nepal or that proposed by Webb (2013) for the Kangra Embayment. Final emplacement of the LHs in the frontal ranges occurred as a result of motion along the MBT. The timing of initiation of motion on the MBT has been assigned to around 11 Ma along the entire Himalayan front (Meigs *et al.*, 1995), although when the first LH rocks were finally exposed at the surface is debated. Deeken *et al.* (2011) have argued that the MBT was active no later than 15 Ma in the area north of our studied sections. Changes in bulk sediment isotopic signature imply that erosion of the ILH had begun in the front ranges by 10–11 Ma in Nepal (Huyghe *et al.*, 2010). Earlier work by Najman *et al.* (2009; 2010) in the same area as our current study indicates that the distinctive ILH were first eroding from the Kullu-Rampur Window by around 11 Ma. Colleps *et al*. (2019) preferred a date for this initial exposure at 3–7 Ma in this NW Indian area, while favoring an older age of 9–11 Ma in Nepal (Fig. 2). Data from the Indus submarine fan records the first significant input from the ILH at ~6 Ma, with a substantial increase around 2–3 Ma (Clift *et al.*, 2019).

In the hinterland to our region of study, the LH are exposed along the range front in the hanging wall of the MBT. It is not always clear whether these units are OLH or ILH. Webb (2013) for example shows undifferentiated LH sedimentary rocks in the hanging wall within the Kangra Embayment and OLH further to the east. Further north ILH are exposed within the tectonic Kullu-Rampur Window (KRW) (Frank *et al.*, 1995) (Figs. 1 and 2) which breaches the GHS and Haimanta. In the KRW, the ILH are composed of amphibolite facies early-mid Proterozoic gneisses, schists and quartzites of the LHCS, which overthrust Mesoproterozoic un-metamorphosed ILH phyllites, quartzites, carbonates and mafic volcanic rocks along the Munsiari Thrust (Valdiya, 1980; Vannay & Grasemann, 1998; Thiede *et al.*, 2004). West of the KRW Haimanta outcrops between the GHS and the range front thrust sheet of LH. According to Vannay *et al*. (2004), after peak metamorphism at ~23 Ma, rapid exhumation of the GHS slowed in this region after around 16 Ma, when movement along the MCT ceased. Peak metamorphic conditions were no older than 11 Ma for the LHCS (Caddick *et al.*, 2007), after which time exhumation occurred along the Munsiari Thrust, with the ILH of the KRW breaching surface in the late Miocene-Early Pliocene (see also Colleps *et al*. (2019)).

3. Summer Monsoon Variations

The NW Himalayas are particularly suitable for testing links between climate and tectonics because the region has one of the best long-term records of climatic evolution in Asia. Moreover, the area is located on the edge of influence of the South Asian summer monsoon (Bookhagen & Burbank, 2006) and thus is particularly sensitive to changes in the intensity and seasonality of the rainfall. Although this area is also supplied by moisture during the winter via the Westerly Jet (Karim & Veizer, 2002), the bulk of the rainfall, and especially the most erosive, stormy precipitation events occur during the summer season (Bookhagen & Burbank, 2006). Summer monsoon precipitation varies across the Indus catchment, broadly decreasing to the west from ~507 mm (76% of the annual total) in Chandigarh (India), to 385 mm (64%) in Islamabad (Pakistan) (www.weather-atlas.com). The Asian monsoon, spanning South and East Asia, is believed to have strengthened due to building of high topography during the Himalayan orogeny (Prell & Kutzbach, 1992; Molnar *et al.*, 1993; Boos & Kuang, 2010), although this may have occurred in a number of phases of uplift and strengthening (Farnsworth *et al.*, 2019). Oceanic upwelling driven by summer monsoon winds seems to have begun to intensify after 13 Ma (Gupta *et al.*, 2015; Betzler *et al.*, 2016), with a subsequent increase after 11 Ma (Bialik *et al.*, 2020) and another at 7–8 Ma (Kroon *et al.*, 1991; Prell *et al.*, 1992).

However, there is a disconnect between oceanic proxies and those related to continental environmental conditions (Clift, 2017). While the transition from C3 tree-dominated flora to a more C4-dominated grassy vegetation around 8 Ma was initially linked to monsoon intensification (Quade *et al.*, 1989), this interpretation has since been reversed to imply Late Miocene drying based on weathering intensity, oxygen isotopes in soil carbonates and the understanding that C4 grasses favor settings with strong dry seasons (Dettman *et al.*, 2001; Vögeli *et al.*, 2017a; Feakins *et al.*, 2020). Hydrogen isotope data from leaf waxes extracted from marine sediments in the Arabian Sea also show a progressive drying since 11 Ma (Huang *et al.*, 2007). This is also consistent with chemical weathering data that demonstrates progressively less intense alteration through time since the Late Miocene in sediments from the Indus Fan (Clift *et al.*, 2008; Clift & Jonell, 2021b; Zhou *et al.*, 2021), although no clear temporal trend was seen in weathering proxies in the sections considered here (Vögeli *et al.*, 2017b). Because chemical weathering rates are generally considered to slow as moisture reduces and temperatures fall (Filippelli, 1997; West *et al.*, 2005), weakening of the monsoon might be expected to cause less chemical weathering and slower erosion, although slower sediment transport would have the opposite effect. The same submarine fan sediments also show increasing amounts of hematite after 10 Ma (Zhou *et al.*, 2021), which is also suggestive of drying environments, or at least increasing seasonality characterized by a prolonged dry season (Schwertmann, 1971).

4. Previous Work

4.1 Foreland Basin Stratigraphy

The Himalayan foreland sedimentary sequence spans much of the Cenozoic. Sections of sedimentary rock from the foreland basin were progressively accreted into the mountains as the Indian plate underthrust northward. Because of this, these sediments are preserved in the Sub-Himalayan Siwalik hills (Fig. 1). Although the oldest part of the basin dates back to the Eocene (Sahni & Srivastava, 1976; Najman, 2006; Ravikant *et al.*, 2011) there is a substantial unconformity separating Paleogene rocks from the overlying Neogene, the latter forming the target of this study (Najman *et al.*, 2004; Najman, 2006). It should be noted that some workers argue for the section being more continuous and without a major break (Bera *et al.*, 2008), although new geochronology data from Colleps *et al*. (2019) casts further doubt on this near continuous age model. The stratigraphic sections exposed at Jawalamukhi and Joginder Nagar form the Sub-Himalayan Neogene succession in our study area within the Kangra Embayment (Fig. 1). The stratigraphic thickness of the Jawalamukhi section is ~3400 m, while the Joginder Nagar section is ~2000 m thick (Fig. 3) (Meigs *et al.*, 1995; Brozovic & Burbank, 2000). Deposition of the Dharamsala Formation in the Kangra Embayment during the Early to Middle Miocene was followed by accumulation of the Middle Miocene to Lower Pleistocene Siwalik Group (Meigs *et al.*, 1995; White *et al.*, 2002). The Joginder Nagar section is made up of the Dharamsala Formation, which contains the Upper and Lower Dharamsala members. The Lower Dharamsala Member comprises the older finer grained Chimnum (>20 Ma) and younger (17–20 Ma) coarser grained Pabo formations (White *et al.*, 2002). The Upper Dharamsala Members comprises an older finer grained Al Formation (15–17 Ma) and a younger coarser Makreri Formation (13–15 Ma). The Jawalamukhi section comprises the Siwalik Group, encompassing the Upper, Middle, and Lower Siwalik sub-groups. The combined sections represent a progressively coarsening-upward sequence represented by fluvial sandstones, mostly of braided river origins passing up into conglomerates of alluvial fan facies (Brozovic & Burbank, 2000; Najman *et al.*, 2009; 2010). The depositional ages of these rocks have been constrained by magnetostratigraphy and radiometric dating of detrital minerals that indicate maximum depositional age, allowing their correlation with climate records (Meigs *et al.*, 1995; White *et al.*, 2001). The younger Jawalamukhi section spans 13–5 Ma and the Joginder Nagar section was deposited at 21–13 Ma (Fig. 3). Combined, these two sections document the longest erosional and exhumation history available in the NW Himalayan foreland (Burbank *et al.*, 1996).

4.2 Earlier Provenance Work from the Joginder Nagar and Jawalamukhi sections

Earlier studies of detrital monazite from the Dharamsala and Lower Siwalik Formations in the Kangra Embayment indicated erosion of both high-grade GHS and similar protoliths such as those preserved in the THS or OLH. The monazite also indicated erosion from Cambro-Ordovician granites now found within the GHS and Haimanta Unit of the THS (White *et al.*, 2001). Further work on the same sections dating to 21–12.5 Ma included petrography, Sr-Nd isotope bulk compositions and single-grain $^{40}Ar/^{39}Ar$ ages of mica (White *et al.*, 2002). This work, particularly the short lag times determined from the predominance of Cenozoic micas, indicated erosion from rapidly cooled GHS sources until ~17 Ma. This was followed by more erosion from a lower grade source following cessation of motion on the MCT, as indicated by influx of older mica grains and change in petrography; this source was considered to be the Haimanta of the THS by White *et al.* (2002), reinterpreted as influx from the OLH by Colleps *et al*. (2019). Colleps *et al*. (2019) used a combination of U-Pb and (U-Th)/He dating of zircons from both the LH and the Dharamsala Group to identify a pulse of rapid exhumation along the Tons Thrust that separates the OLH from the ILH at ~16 Ma. After ~12 Ma duplexing of the ILH shifted the locus of maximum exhumation northward, allowing the rocks in the MCT hanging wall to be eroded and exposing the ILH in the KRW. The upper part of the foreland sedimentary succession postdating 13 Ma near Jawalamukhi was analyzed using the same methods by Najman *et al*. (2009; 2010). This work implied initial erosion of the non-metamorphosed ILH after 11 Ma, based on the ε_{Nd} values of clasts in pebbly sandstones; then loss of GHS drainage with material predominantly derived from the Haimanta starting at 7 Ma, based on loss of Cenozoic micas; and then erosion from the LHCS after 6 Ma based on a change to dominance of Precambrian micas.

Further to the east a multi-proxy study involving U-Pb zircon dating, bulk sediment geochemistry and Sr-Nd isotopes targeted the Siwalik Group in the Dehra Dun region (Mandal *et al*., 2019). This work concluded that LHCS erosion started after 6 Ma, following ILH erosion starting at least since 10 Ma, although erosion from the GHS and THS dominated. Erosion and recycling of foreland sedimentary rocks intensified after 5.5 Ma probably because of southward propagation of the thrust front from the MBT.

4.3 Rivers

The Indus River and its many tributaries are the main drainage system in the NW Himalayan foreland (Fig. 2). The Beas River is an important tributary for this study because it is located close to the sampled outcrops. Because the Siwaliks are offscraped and accreted parts of the foreland the preserved sections must represent older equivalents of the modern floodplain, potentially related to the Beas River since ongoing convergence necessarily brings Beas River deposits towards the location of the preserved sections, where they might be offscraped in the future, although axial rivers flowing further south might also be expected to contribute to older parts of the preserved section. Although it has been argued that the eastern tributaries of the Indus River used to flow to the east prior to the Late Miocene (Clift & Blusztajn, 2005), this model has been questioned because it does not account for changing compositions through time of the individual streams (Chirouze *et al.*, 2015).

5. Methods

13 sandstones were sampled from the Jawalamukhi and Joginder Nagar sedimentary sections as shown in Figures 2 and 3, spanning the time range from 21 to 5 Ma (Table 1). We also sampled the Beas River for a modern river sand for apatite fission track (AFT) work only. We use a selection of bulk rock and single grain methods in order to constrain the source of the sediments. Using a combination of different proxies allows the sediment source to be more accurately defined and overcomes limitations in the resolution of individual methods. We use both high and low temperature geo- and thermochronology to resolve between erosion from different source ranges, as well as integrating pre-existing thermochronology and isotopic data taken from the same section.

5.1 X-Ray Fluorescence (XRF)

Although erosion and sediment transport may result in changes in the bulk sediment chemistry of deposited sediments compared with the pristine source rocks, major and trace element chemistry of sedimentary rocks can be used to constrain their origin because some elements are resistant to alteration and mobilization during diagenesis (McLennan *et al.*, 1993; Fedo *et al.*, 1995; Singh, 2009). These data may also provide an image of the state of chemical weathering through the section (Nesbitt *et al.*, 1980), which in turn may be linked to the monsoon climate. The major element chemistry can show us large scale changes in sediment character that provide context for the geochronology described below.

All thirteen whole rock sandstone samples were cut and processed through a jaw crusher. The crushed rock samples were milled into fine grained powders. The powders were analyzed for a suite of major elements and select trace elements through XRF spectrometry by the Washington State University (WSU) GeoAnalytical Laboratory. Full analytical details are provided by Johnson *et al*. (1999). Analytical uncertainties for major elements are ~1% of the measured value, as determined from repeat analysis of a suite of nine USGS standard samples. Results are provided in Table 2.

5.2 U-Pb Detrital Zircon Dating

Detrital zircon U-Pb dating was completed using laser ablation-multicollector-inductively coupled plasma-mass spectrometry (LA-MC-ICP-MS). After separation of the zircon fraction by standard heavy liquid methods by GeoSep Services of Moscow Idaho, the grains were mounted and the U-Th-Pb isotopic compositions were determined at the London Geochronology Centre facilities at University College London using a New Wave 193 nm aperture-imaged, frequency-quintupled laser ablation system, coupled to an Agilent 7900 quadrupole-based ICP–MS. Full methodology can be found in the Supplementary Information, along with all the isotopic analytical data in Table S1.

We used kernel density estimates (KDEs) with pie charts to graphically display the detrital age spectra and a multi-dimensional scalar (MDS) diagram to assess the degree of similarity between samples (Vermeesch, 2013). Further modelling of the source contributions was made using the DZMix Matlab routine of Sundell & Saylor (2017). This involves a Monte Carlo-based mixing model, which allows the defined sources to the basin to be combined in order to try and replicate the age spectra measured for each of the samples. 10,000 attempts are made to replicate each particular detrital age spectrum through varying the contributions from the various sources in order to match the observed age spectrum, with the best 1% selected (Figs. S1 and S2; Table S2 in Online Supplement). This type of mixing can only be as good as the definition of the source areas, although a large amount of bedrock data exists for the Himalayas. The ILH is distinctly different from the OLH, THS and GHS concerning its U-Pb age spectrum. Because the OLH is the protolith to the GHS, these two sources are indistinguishable in terms of their zircons age spectra. The younger THS has a slightly different signature than the GHS and OLH, for example having a more prominent ~500 Ma population and slightly fewer 900–1250 Ma grains, but it is mostly sourced from these older units and therefore the differences are subtle. Therefore, we combine the OLH, GHS and THS sources into one end member to allow a robust mixing model to be generated.

Furthermore, there is the added complexity that material that was originally derived from one basement source might have been eroded and deposited temporarily elsewhere from where it was then reworked into the flood plains (e.g., from the older Dharamsala Formation). Recycling material out of older sedimentary sequences complicates the sediment unmixing and is known to affect the modern rivers (Clift & Jonell, 2021a); however, quantitative estimates from the Nepalese central Himalaya indicate that the load of the rivers in that area contains no more than ~10% material recycled from the Siwalik Group (Lavé & Avouac, 2000). We thus do not include these sedimentary rocks in our mixing models, because Siwalik end members cannot be used to model other Siwalik sedimentary rocks. There is no simple way to remove this recycling effect, but it might be expected to influence all our samples. We look for systematic major changes in zircon age populations to quantify changes in provenance with the understanding that even apparently unique peaks might be recycled through older sedimentary deposits.

5.3 Apatite Fission Track

We use AFT methodology to trace the exhumation history of the source region by looking at how lag times (mineral cooling age minus depositional age) evolve through the section. The approach has been effective at reconstructing erosion rates elsewhere in the Himalaya. Analysis of AFT in Nepal suggested that parts of the section may be reset during burial, prior to later uplift and exposure (van der Beek *et al.*, 2006). Studies of fission track in the Siwaliks of the NW Himalayas have largely been restricted to zircon FT (Bernet *et al.*, 2006; Chirouze *et al.*, 2015), although AFT data spanning the last 16 Ma is available for comparison from the Indus Fan (Zhou *et al.*, 2020).

AFT data were collected from eight samples ranging from 5–19 Ma plus as well a single modern river sand from the Beas River. Following mineral separation AFT analysis was performed at the London Geochronology Centre using the external detector approach Full methods can be found in Supplementary Information.

6. RESULTS

6.1 Major Element Chemistry

The major element chemistry indicates that these sediments are typical high SiO_2 sandstones ranging from 66.6% to 93.3%, average 80.8% SiO_2 after normalizing for volatile content (Fig. 4). This compares with an average of 74.9% SiO_2 for modern Indus catchment Himalayan tributaries. The sediments have low contents of water mobile alkali earth elements, such as K_2O and Na_2O. Average contents are 1.84% and 0.75% respectively compared with 2.38% and 1.06% for the modern tributaries (Alizai *et al.*, 2011). On the ternary plot of Fedo *et al.* (1995)(Fig. 4A), the samples overlap with the analyses of Vögeli *et al.* (2017b) for the same sections but show a coherent displacement to higher Chemical Index of Alteration (CIA) values compared to the Quaternary Indus delta, shelf and canyon (Clift *et al.*, 2010; Li *et al.*, 2018), as well as post 11 Ma turbidites from the Indus Fan (Zhou *et al.*, 2021). The sediments yield very high Zr contents, averaging 209 ppm compared to 38 ppm for the modern rivers, with the nearest streams, the Sutlej and the Beas, having only ~14 ppm (Alizai *et al.*, 2011). The contrast with the Quaternary and older Indus Fan sediments is also clear on the diagram of Herron (1988) in which the samples first analyzed in this study plot as arkose to sublitharenite rather than as wackes.

6.2 Detrital U-Pb Zircon

The age spectra of the detrital grains show a number of repeated common age populations that are comparable to ages measured from basement source rocks (Fig. 5). The most common populations range 400–750 Ma, 900–1250 Ma, 1700–2000 Ma and >2400 Ma. Grains deposited at and before 8–9 Ma are dominated by the 750–1250 Ma population. There is little variation in age composition from 20 to 11 Ma, although the oldest two samples deposited at 18–19 Ma and 20–21 Ma show very few 400–750 Ma grains. The zircon age spectra over the interval before 11 Ma are most similar to the OLH, THS and GHS, and the modern Ravi River (Figs. 5 and 6). After 12 Ma, samples show an appreciable increase in zircons in the range 1700–2000 Ma (Fig 5), typical of the ILH, and samples younger than 8 Ma are distinctive in having a strong 1800–1900 Ma peak and very few grains younger than 1700 Ma, similar to the modern Sutlej River, but unlike the Beas River. None of the samples contain grains <200 Ma, which are associated with the Indus River and to a lesser extent the Jhelum River (where the grains span ~10–200 Ma and are derived from the Karakoram, Kohistan and Nanga Parbat (Alizai *et al.*, 2011)), or even grains dated ~30 Ma which are common in the Siwalik Group at Dehra Dun, as well as the Ganges (Mandal *et al.*, 2019). Given the lack of 30–200 Ma grains in our section, these 30 Ma zircons must come from

Oligocene intrusive rocks in the GHS which are uncommon in NW India west of Dehra Dun (Steck, 2003)

6.3 Apatite Fission Track

The central age defined by the radial plots (Fig. S1 in Online Supplement) represents the time at which the dominant bedrock sources cooled through the AFT partial annealing zone (PAZ), assuming that the sedimentary rock itself has not been subjected to temperatures sufficient for the AFT ages to be reset, since deposition. The Beas River sample is clearly not reset and has a central age of 1.4 ± 0.1 Ma, dominated by a single population (Table 3). The four youngest sedimentary rocks (5–9 Ma) yielded single AFT populations indicating very short lag times (central ages within error of their depositional age; Fig. 7). AFT analysis showed that samples older than 9–10 Ma have been partially to completely reset because (1) their central age is significantly younger than their depositional age, and (2) the central age youngs down section, which is typical of a reset section.

7 Discussion

7.1 Major Element Chemistry

The major element chemistry is consistent with erosion from typical upper continental crustal sources, although the contrast with the modern rivers and with the older deposits in the Arabian Sea indicates that these sedimentary rocks are generally more weathered than the sediments that reached the final depocentre in the recent or older past. The greater degree of alteration reflects both their long storage in the floodplains immediately after sedimentation, when they would have been exposed to moisture and heat, as well as renewed alteration during diagenesis and further weathering as the ranges were uplifted more recently and the sediments were again exposed. The high proportion of Zr compared to the modern rivers is suggestive of the sources being relatively enriched in zircon compared to other source regions within the Indus catchment, especially those in the suture zone and Karakoram. Strong weathering and diagenesis may also have broken down less robust phases and increased the proportion of zircon. The major element chemistry is however not diagnostic in terms of limiting the bedrock sources.

7.2 Detrital U-Pb Zircon

As noted above (see Section 6.2), for samples deposited from 21–9 Ma the dominant population (750–1250 Ma) is similar to those seen in the OLH, GHS and THS (Fig. 5), which share a very similar zircon U-Pb signature (see Section 5.2). It is clear that most of the samples are similar to one another and distinct from the Indus River and the ILH (Fig. 6 and S4). Because the Indus derives its sediments largely from the Karakoram and other parts of the suture zone (Garzanti *et al.*, 2005; Garzanti *et al.*, 2020), the contrast with a part of the Himalayan foreland remote from the Indus mainstream is unsurprising.

7.2.1 Transition after 11 Ma

At 11–12 Ma there was an increase in the 1700–2000 Ma zircon population distinctive of the ILH, with further increase up-section, especially after 8 Ma (Fig. 5). End member modelling using DZMix also supports the relative increase in erosion from the ILH, starting after 11 Ma and accelerating after 8 Ma (Fig. 8a). Although 1700–2000 Ma grains are also seen in the OLH, GHS and THS they are relatively scarce in those rocks compared to 750–1250 Ma zircons. If these latter units were sources of the increase in 1700–2000 Ma grains to the Jawalamukhi section, then we would anticipate finding far greater proportions of zircons of this younger 750–1250 Ma population; however, this is not the case. Input from the ILH starting from 11 Ma is consistent with previous work in this area, which identified non-metamorphosed ILH input from the Nd isotopic signature of pebbly sandstone clasts by that time (Najman *et al.*, 2010) (Fig. 8b). However, this previous work was unable to determine relative proportions of such input as it was based on clast data, unrepresentative of the section overall.

Moreover, this age is consistent with the evidence for ILH erosion obtained slightly further to the east in the Dehra Dun area where zircons indicate initial unroofing of these units at least since 10 Ma (Mandal *et al.*, 2019).

7.2.2 Transition after 8 Ma

The distinct increase in 1700–2000 Ma zircons at 7–8 Ma (Fig. 5), tracking towards the ILH on the MDS plot (Fig. 6A) is coincident with the loss of mica grains dated <50 Ma (Najman *et al.*, 2009), implying loss of erosion from the GHS. Dominance of Paleozoic and Mesozoic micas at this time would suggest a continuing Haimanta contribution in addition to the ILH (Fig. 8e). A second switch in mica provenance by 6 Ma, when grains become entirely Precambrian, and a major change in Sr-Nd values of bulk sediment to values typical of the ILH (Fig 8b), is consistent with a major ILH contribution, as indicated by the zircon ages.

It is important to note that the OLH are not exposed in the Kangra Embayment or in the KRW and are not drained by the Beas River. It is thus unlikely that the Siwalik sections would have received sediment from OLH sources close to the range front. Sediment supply to the sections must have been from a paleo-Sutlej, Beas or potentially a smaller local river.

In the Dehra Dun area there was no loss of erosion from the GHS as we see at Jawalamukhi, implying that this section was deposited from a separate river. Figure 9 shows KDE plots of synchronous of samples from the Mohand Rao section at Dehra Dun and the Jawalamukhi section. The figure shows that the size of the populations between 400 and 1250 Ma remained high at Dehra Dun after 8 Ma while these groupings contracted sharply at Jawalamukhi.

7.2.3 Causes of the Provenance Changes

The changes in provenance could reflect autogenic drainage reorganization in the flood plain, and/or the motion of the section across the basin between different river flood plains. Alternatively, changes in provenance could relate to the progressive unroofing of the KRW and the addition of ILH material to this area.

Tectonic evolution of the region, as determined from bedrock data, may well explain the provenance changes we observe in the foreland. Prograde metamorphism in the LHCS of the KRW terminated at 11 Ma by tectonic exhumation along the Munsiari Thrust (Vannay *et al.*, 2004; Caddick *et al.*, 2007; Thiede *et al.*, 2009). Najman *et al.* (2009; 2010) interpreted the first appearance of ILH material at 11 Ma in the Jawalamukhi section as the result of input of non-metamorphosed ILH material associated with this exhumation event, followed by exhumation of the LHCS by 6 Ma, as unroofing of the window progressed. This is in agreement with the interpretation of Mandal *et al.* (2019), in which a provenance change in the Siwalik Group at Dehra Dun at 6 Ma is interpreted as due to unroofing of the LHCS.

Alternatively, provenance evolution may reflect changes in the location of the sites relative to the foreland rivers (Fig. 10). India has been moving towards the NNE throughout the Neogene (Molnar & Stock, 2009; Copley *et al.*, 2010; Clark, 2012) and as a result each of the sections that have been accreted into the thrust stack within the Kangra Embayment must have approached this part of the thrust front from the SSW prior to their offscraping. The rate of convergence (Clark, 2012) and the estimated distance of each section at the time of sedimentation of the individual samples are provided in Table 1 and can be used as a rough guide to where each sample was deposited relative to the mountain front. Stevens & Avouac (2015), estimate that presently around half of the total convergence between India and Eurasia is absorbed within the Himalaya, so we make an approximation that the other half represents convergence between the foreland basin and the mountain front, in order to reposition each of the samples at the time of their sedimentation.

We estimate the geology of the source areas at various critical times based on the geological map of DiPietro & Pogue (2004). Although we use the structural reconstructions of Colleps *et al*. (2019) as a guide to the progressive unroofing of the different basement units, we adjust these models for unroofing based on the results of our provenance analysis, as set out above.

As each section moved towards the Himalayas with ongoing convergence, each section would have been under the influence of different rivers with contrasting provenance at different times (Fig. 10). The major rivers flow towards the SW and when the sites were in the distal foredeep, far from the mountain front, they may have been affected by sedimentation from these tributaries. As they got closer to the mountains, in the proximal foredeep, each section would have the opportunity to be affected by more local rivers (e.g., the Beas), which themselves would have been in a state of constant reorganization and migration.

Sediment older than 11 Ma was supplied by a river eroding the GHS and THS, similar to the modern Ravi River. However, the Ravi drainage has evolved since this time and the direction of flow from its NW location precludes this as being the source of the older sediments at Jawalamukhi and Joginder Nagar. The location of the Sutlej makes it the most likely source of sediment, although the provenance signature must have been quite different than the LH dominance seen in the modern Sutlej (Alizai *et al.*, 2011). This is to be expected since the KRW that dominates the modern river was not yet exposed at that time.

We infer that the younger part of the section is being supplied by a river which was dominantly deriving its material from the ILH, probably related to the KRW. The MDS plot (Fig.

6) shows the younger samples are most like the modern Sutlej. It is noteworthy that the Sutlej River basin contain significant exposures of the GHS and THS but has a zircon population dominated by ILH sources because of climatically driven focused erosion (Alizai *et al.*, 2011). Nevertheless, the ε_{Nd} value of the modern Sutlej (Clift *et al.*, 2002) indicates that there is a proportion of material derived from the GHS or THS; therefore, because the detrital mica data shows that GHS material was cut from the younger part of Jawalamukhi section (Najman *et al.*, 2009; 2010), it is more likely that the younger sediments of the Jawalamukhi section would have been supplied by a small local river draining only as far as the KRW or the neighboring Uttarkashi semi-window. The provenance transition after 8 Ma may reflect motion from the Sutlej flood plains to the Beas flood plains. If it was the Beas River then this must have changed its provenance significantly since 5–6 Ma.

7.2.4 Comparison with the Indus Fan

From this set of detrital zircon data, combined with previously published techniques, it can be deduced that the unroofing of the ILH in the source regions to these sediments began by 11 Ma and increased after 8 Ma. Prior to that time the foreland deposits at Jawalamukhi are mostly derived from the GHS and/or THS (Haimanta), since at least ~21 Ma. Relative lack of 1700–2000 Ma zircons seen in the Indus submarine fan until ~2 Ma (Clift *et al.*, 2019), implies that most of the Indus catchment had not exposed significant ILH bedrock until much later than inferred at Jawalamukhi. Thus, the river that supplied the sediments we study from 11 to 2 Ma was deriving its material from a catchment that was atypical of the wider area to the NW, or that its discharge was greatly diluted by supply from contrasting rivers that were not so greatly eroding ILH sources. The foreland sediments dated here between 11–2 Ma were however more similar to foreland sediments found in the Dehra Dun area further east in showing major erosion from the ILH after

11 Ma (Mandal *et al.*, 2019) compared to those in the Indus Fan. Sediments at Dehra Dun differ from Jawalamukhi in retaining a significant GHS and THS input since at least 11 Ma.

7.3 Apatite Fission Track

Figure 7 shows how the AFT ages of the samples measured in this study compare both with their depositional ages, and with other data both further east in the Nepalese part of the foreland basin, as well as in the Indian Ocean submarine fans. There is no suggestion of more than one AFT age population in those samples (8–9 Ma, 6–7 Ma, and 5–6 Ma), whose central ages are within error of the depositional age, and therefore not reset. Their younging up-section is typical of erosion from a progressively exhuming hinterland. These samples have short lag times indicating rapid exhumation of the source region.

By contrast, samples older than 9 Ma are considered to be reset because the AFT ages form a single population with a central age resolvably younger than the depositional age derived from magnetic stratigraphy. Most of the reset rocks in the oldest part of the Joginder Nagar section lie in the hanging wall of the Palampur Thrust that initiated prior to the oldest reset age of ~7 Ma. This is consistent with the idea that the Dharamsala Formation and Lower Siwalik section (Joginder Nagar section) was accreted to the toe of the orogenic wedge after 11.5 Ma, which is the age of the youngest sediment known from this section. We conclude that the Palampur Thrust must have started motion between 7.0 and 11.5 Ma. The single reset 2.2 Ma AFT age south of the Palampur Thrust reflects an episode of uplift and erosion of that section by 2.2 Ma, presumably on the MFT or an associated splay.

The AFT ages themselves do not provide any provenance information, because bedrock AFT data from the potential sources in the modern mountains do not allow us to infer what the AFT ages were in the same ranges in the past. Although we cannot determine the timing of the start of rapid exhumation because the older samples are reset, it is noteworthy that the occurrence of very rapidly cooled sediments starting no later than 9–10 Ma encompasses the time of increasing flux of ILH materials into the basin we study. Earlier studies suggest that erosion of the THS and GHS was slower after ~16–17 Ma in this region (White *et al.*, 2001; Vannay *et al.*, 2004; Thiede *et al.*, 2009), albeit getting faster again in the Dhauladar Range of Chamba after the start of motion on the MBT after ~10 Ma (Deeken *et al.*, 2011; Thiede *et al.*, 2017). Our data support the idea of rapid unroofing of the duplexed ILH and LHCS in the KRW starting at least by the Late Miocene (~11 Ma), and particularly after 9 Ma, consistent with bedrock data from the ILH in the KRW (Caddick *et al.*, 2007; Thiede *et al.*, 2009; Schlup *et al.*, 2011). Modelling of thermochronology data from the Sutlej-Beas region suggests accelerating erosion from the KRW after 7 Ma (Stübner *et al.*, 2018). We further note that this was a time of rapid regional exhumation, as inferred from AFT studies of the Indus submarine fan (Zhou *et al.*, 2020), the Bengal Fan (Huyghe *et al.*, 2020), as well as in the Nepalese part of the foreland (Bernet *et al.*, 2006; van der Beek *et al.*, 2006). Lag times are longer in the modern Beas River than in the foreland sediment deposited between 9 and 6 Ma but because the sources are quite different from the youngest Siwalik sedimentary rocks in this study (Fig. 6) we cannot infer a widespread slowing of exhumation in this region since 5–6 Ma based on these new data.

8. Climate-Tectonic Synthesis

The relative importance of tectonics versus climate in the evolution of the Himalayas is long-debated, with the relative influence of variations in thrust belt geometry and its implications for topographic development and landsliding, versus wetter climates and associated increase in erosion both cited as important controls (Robert *et al.*, 2011; Thiede & Ehlers, 2013; Godard *et al.*, 2014).

Rapid exhumation of the ILH duplex since 11 Ma, may be explained solely by tectonics which could have driven surface uplift and so facilitated mass wasting on steep slopes (Mandal *et al.*, 2019). River incision of the ILH in the KRW may be linked to solid Earth tectonic processes, for example the ramp geometry of the Main Himalayan Thrust (Eugster *et al.*, 2018; Colleps *et al.*, 2019). However, the substantial increase of ILH input after 8 Ma is also coincident with a time of climatic transition (Quade *et al.*, 1989; Singh *et al.*, 2011). In the foreland basin there is a transition from C3 tree-dominated to a C4 grass-dominated vegetation at this time interpreted to reflect a general drying of the climate, or at least the development of a strong dry season (Dettman *et al.*, 2001; Feakins *et al.*, 2020). This trend was confirmed in the sections studied here by Vögeli *et al*. (2017a) indicating a climatic transition at 7–8 Ma involving drying and more seasonality in the NW Himalayas after that time,which is a hallmark of the South Asian monsoon.

Various proxies suggest that the region was drying in the Late Miocene and that both regional weathering and erosion were slowing in the Indus Basin as a result (Clift *et al.*, 2008; Clift, 2017). However, that is not to say that more limited parts of the mountain front were experiencing rapid erosion, especially the LH (Caddick *et al.*, 2007; Thiede *et al.*, 2009). It is possible that the climate change would have caused the maximum rainfall band to migrate southwards compared to its location when the summer monsoon was stronger and rain penetrated deeper into the Himalayas during the Middle and Early Miocene. If climate was an important driver of exhumation, we suggest a feedback whereby uplift caused by thrusting in the LH wedge focused the rainfall by generating topography that focused orographic rainfall and allowed the LH duplex to further build and then exhume (Thiede & Ehlers, 2013). This contrasts with the area further NW in Chamba where the high ranges of the GHS form a rain shadow, reduce erosion and prevent duplexing of the underlying ILH (Deeken *et al.*, 2011).

9. Conclusions

Our study highlights the importance of localized foreland sections to accompany regional erosional reconstructions, which are based on submarine fan sequences, when trying to understand the erosion of large mountain belts over tectonically significant periods of geological time (>10 m.y.). Our work is consistent with the idea of ongoing climate-tectonic coupling. While stronger monsoon may have driven exhumation of the GHS, the weakening and migration of rainfall in the Late Miocene could be associated with duplexing.

Evidence for appreciable erosion from the ILH starts around 11 Ma and increased progressively after 8 Ma. ILH input after 11 Ma is consistent with timing of movement on the MBT, as well as with onset of ILH duplexing. Najman *et al*. (2009; 2010) attributed the change from 8 Ma to progressive uplift and unroofing of the rocks in the KRW, consistent with the timing of the window's exhumation as determined from bedrock analyses (Colleps *et al.*, 2019). The loss of GHS and Haimanta erosion could indicate drainage evolution in the foreland and supply from a smaller river late in the accumulation of the section. Progressive motion of the Jawalamukhi section towards the range front, and/or drainage reorganization in the foreland during the Late Miocene may play a role in controlling which river was supplying the section prior to its accretion into the toe of the orogenic wedge.

The Jawalamukhi section must have initially been in the floodplains of a major, likely basin axial river which was eroding both LH rocks and GHS-THS sources, probably a paleo-Sutlej. Both modern rivers are dominated by grains of LH origin (Alizai *et al.*, 2011) despite the fact that GHS and THS rocks are widely exposed in their catchments. However, the almost complete lack of Cenozoic micas in the youngest sediments suggests that a smaller transverse river with no GHS/THS source is more appropriate.

621

Acknowledgements

PC is grateful for support from the Charles T. McCord Chair in Petroleum Geology at Louisiana State University. GeoSep Services are thanked for their mineral separating. Data for this paper are available from Mendeley Data (https://data.mendeley.com), doi: 10.17632/9gjmpbc443.1. Andrew Carter performed the zircon dating and fission track analysis. Yani Najman collected the sample. Elise Exnicios processed the samples. Peter Clift and Elise Exnicios made the figures and wrote the initial draft to which Yani Najman contributed. Peter Clift and Yani Najman wrote the revised draft. All authors contributed to the interpretation and final manuscript. The paper benefited from review comments from Rasmus Thiede and an anonymous reviewer.

REFERENCES

Aitchison, J.C., Ali, J.R. & Davis, A.S. (2007) When and Where Did India and Asia Collide? *Journal of Geophysical Research*, **112**. doi:10.1029/2006JB004706.

Alizai, A., Carter, A., Clift, P.D., VanLaningham, S., Williams, J.C. & Kumar, R. (2011) Sediment Provenance, Reworking and Transport Processes in the Indus River by U–Pb Dating of Detrital Zircon Grains. *Global and Planetary Change*, **76,** 33-55. doi:10.1016/j.gloplacha.2010.11.008.

Badgley, C. & Tauxe, L. (1990) Paleomagnetic Stratigraphy and Time in Sediments: Studies in Alluvial Siwalik Rocks of Pakistan. *The Journal of Geology*, **98,** 457-477. doi:10.1086/629419.

Beaumont, C., Jamieson, R.A., Nguyen, M.H. & Lee, B. (2001) Himalayan Tectonics Explained by Extrusion of a Low-Viscosity Crustal Channel Coupled to Focused Surface Denudation. *Nature*, **414,** 738-742. doi:10.1038/414738a.

Bera, M.K., Sarkar, A., Chakraborty, P.P., Loyal, R.S. & Sanyal, P. (2008) Marine to Continental Transition in Himalayan Foreland. *Geological Society of America Bulletin*. doi:10.1130/B26265.1.

Bernet, M., van der Beek, P., Pik, R., Huyghe, P., Mugnier, J.-L., Labrin, E. & Szulc, A.G. (2006) Miocene to Recent Exhumation of the Central Himalaya Determined from Combined Detrital Zircon Fission-Track and U/Pb Analysis of Siwalik Sediments, Western Nepal. *Basin Research*, **18,** 393–412. doi: 10.1111/j.1365-2117.2006.00303.

Betzler, C., Eberli, G.P., Kroon, D., Wright, J.D., Swart, P.K., Nath, B.N., Alvarez-Zarikian, C.A., Alonso-García, M., Bialik, O.M., Blättler, C.L., Guo, J.A., Haffen, S., Horozai, S., Inoue, M., Jovane, L., Lanci, L., Laya, J.C., Mee, A.L.H., Lüdmann, T., Nakakuni, M., Niino, K., Petruny, L.M., Pratiwi, S.D., Reijmer, J.J.G., Reolid, J., Slagle, A.L., Sloss, C.R., Su, X., Yao, Z. & Young, J.R. (2016) The Abrupt Onset of the Modern South Asian Monsoon Winds. *Scientific Reports*, **29838**. doi:10.1038/srep29838.

Bialik, O.M., Auer, G., Ogawa, N.O., Kroon, D., Waldmann, N.D. & Ohkouchi, N. (2020) Monsoons, Upwelling, and the Deoxygenation of the Northwestern Indian Ocean in Response to Middle to Late Miocene Global Climatic Shifts. *Paleoceanography and Paleoclimatology*, **35,** e2019PA003762. doi:10.1029/2019PA003762.

Bollinger, L., Avouac, J.P., Beyssac, O., Catlos, E.J., Harrison, T.M., Grove, M., Goffe, B. & Sapkota, S. (2004) Thermal Structure and Exhumation History of the Lesser Himalaya in Central Nepal. *Tectonics*, **23,** 19. doi:10.1029/2003TC001564.

Bookhagen, B. & Burbank, D.W. (2006) Topography, Relief, and Trmm-Derived Rainfall Variations Along the Himalaya. *Geophysical Research Letters*, **33**. doi:10.1029/2006GL026037.

Boos, W.R. & Kuang, Z. (2010) Dominant Control of the South Asian Monsoon by Orographic Insulation Versus Plateau Heating. *Nature*, **463,** 218-222. doi:10.1038/nature08707.

Brookfield, M.E. & Andrews-Speed, C.P. (1984) Sedimentology, Petrography and Tectonic Significance of the Shelf, Flysch and Molasse Clastic Deposits across the Indus Suture Zone, Ladakh, Nw India. *Sedimentary Geology*, **40,** 249-286. doi:10.1016/0037-0738(84)90011-3.

Brozovic, N. & Burbank, D.W. (2000) Dynamic Fluvial Systems and Gravel Progradation in the Himalayan Foreland. *GSA Bulletin*, **112,** 394-412. doi:10.1130/0016-7606(2000)112<394:Dfsagp>2.0.Co;2.

Burbank, D.W., Beck, R.A. & Mulder, T. (1996) The Himalayan Foreland Basin. In: *The Tectonics of Asia* (Ed. by A. Yin & T. M. Harrison), 149–188. Cambridge University Press, New York.

Caddick, M.J., Bickle, M.J., Harris, N.B.W., Holland, T.J.B., Horstwood, M.S.A., Parrish, R.R. & Ahmad, T. (2007) Burial and Exhumation History of a Lesser Himalayan Schist: Recording the Formation of an Inverted Metamorphic Sequence in Nw India. *Earth and Planetary Science Letters*, **264,** 375-390. doi:10.1016/j.epsl.2007.09.011.

Cawood, P.A., Johnson, M.R.W. & Nemchin, A.A. (2007) Early Palaeozoic Orogenesis Along the Indian Margin of Gondwana: Tectonic Response to Gondwana Assembly. *Earth and Planetary Science Letters*, **255,** 70-84. doi:10.1016/j.epsl.2006.12.006.

Célérier, J., Harrison, T.M., Webb, A.A.G. & Yin, A. (2009) The Kumaun and Garwhal Lesser Himalaya, India: Part 1. Structure and Stratigraphy. *GSA Bulletin*, **121,** 1262-1280. doi:10.1130/b26344.1.

Chirouze, F., Huyghe, P., Chauvel, C., van der Beek, P., Bernet, M. & Mugnier, J.-L. (2015) Stable Drainage Pattern and Variable Exhumation in the Western Himalaya since the Middle Miocene. *Journal of Geology*, **123,** 1–20. doi:10.1086/679305.

Clark, M.K. (2012) Continental Collision Slowing Due to Viscous Mantle Lithosphere Rather Than Topography. *Nature*, **483,** 74-77. doi:10.1038/nature10848.

Clift, P.D., Shimizu, N., Layne, G., Gaedicke, C., Schlüter, H.U., Clark, M.K. & Amjad, S. (2001) Development of the Indus Fan and Its Significance for the Erosional History of the Western Himalaya and Karakoram. *Geological Society of America Bulletin*, **113,** 1039–1051. doi:10.1130/0016-7606(2001)113<1039:DOTIFA>2.0.CO;2.

Clift, P.D., Lee, J.I., Hildebrand, P., Shimizu, N., Layne, G.D., Blusztajn, J., Blum, J.D., Garzanti, E. & Khan, A.A. (2002) Nd and Pb Isotope Variability in the Indus River System; Implications for Sediment Provenance and Crustal Heterogeneity in the Western Himalaya. *Earth and Planetary Science Letters*, **200,** 91-106. doi:10.1016/S0012-821X(02)00620-9.

Clift, P.D. & Blusztajn, J.S. (2005) Reorganization of the Western Himalayan River System after Five Million Years Ago. *Nature*, **438,** 1001-1003. doi:10.1038/nature04379.

Clift, P.D., Hodges, K., Heslop, D., Hannigan, R., Hoang, L.V. & Calves, G. (2008) Greater Himalayan Exhumation Triggered by Early Miocene Monsoon Intensification. *Nature Geoscience*, **1,** 875-880. doi:10.1038/ngeo351.

Clift, P.D., Giosan, L., Carter, A., Garzanti, E., Galy, V., Tabrez, A.R., Pringle, M., Campbell, I.H., France-Lanord, C., Blusztajn, J., Allen, C., Alizai, A., Lückge, A., Danish, M. & Rabbani, M.M. (2010) Monsoon Control over Erosion Patterns in the Western Himalaya: Possible Feed-Backs into the Tectonic Evolution. In: *Monsoon Evolution and Tectonic-Climate Linkage in Asia* (Ed. by P. D. Clift, R. Tada & H. Zheng), *Special Publication*, **342**, 181–213. Geological Society, London.

Clift, P.D. (2017) Cenozoic Sedimentary Records of Climate-Tectonic Coupling in the Western Himalaya. *Progress in Earth and Planetary Science,* **4**. doi:10.1186/s40645-017-0151-8.

Clift, P.D., Zhou, P., Stockli, D.F. & Blusztajn, J. (2019) Regional Pliocene Exhumation of the Lesser Himalaya in the Indus Drainage. *Solid Earth*, **10,** 647-661. doi:10.5194/se-10-647-2019.

Clift, P.D., Kulhanek, D.K., Zhou, P., Bowen, M.G., Vincent, S.M., Lyle, M. & Hahn, A. (2020) Chemical Weathering and Erosion Responses to Changing Monsoon Climate in the Late Miocene of Southwest Asia. *Geological Magazine*, **157,** 939-955. doi:10.1017/S0016756819000608.

Clift, P.D. & Jonell, T.N. (2021a) Monsoon Controls on Sediment Generation and Transport: Mass Budget and Provenance Constraints from the Indus River Catchment, Delta and Submarine Fan over Tectonic and Multi-Millennial Timescales. *Earth-Science Reviews***,** 103682. doi:10.1016/j.earscirev.2021.103682.

Clift, P.D. & Jonell, T.N. (2021b) Himalayan-Tibetan Erosion Is Not the Cause of Neogene Global Cooling. *Geophysical Research Letters*, **n/a,** e2020GL087742. doi:10.1029/2020GL087742.

Colleps, C.L., Stockli, D.F., McKenzie, N.R., Webb, A.A.G. & Horton, B.K. (2019) Neogene Kinematic Evolution and Exhumation of the Nw India Himalaya: Zircon Geo- and Thermochronometric Insights from the Fold-Thrust Belt and Foreland Basin. *Tectonics*, **38,** 2059-2086. doi:10.1029/2018tc005304.

Copley, A., Avouac, J.-P. & Royer, J.-Y. (2010) The India-Asia Collision and the Cenozoic Slowdown of the Indian Plate; Implications for the Forces Driving Plate Motions. *Journal of Geophysical Research*, **115**. doi:10.1029/2009JB006634.

Corrigan, J.D. & Crowley, J.L. (1990) Fission Track Analysis of Detrital Apatites from Sites 717 and 718, Leg 116, Central Indian Ocean. *Proceedings of the Ocean Drilling Program, Scientific Results*, **116,** 75–92. doi:10.2973/odp.proc.sr.116.118.1990.

Curray, J.R., Emmel, F.J. & Moore, D.G. (2003) The Bengal Fan: Morphology, Geometry, Stratigraphy, History and Processes. *Marine and Petroleum Geology*, **19,** 1191–1223. doi:10.1016/S0264-8172(03)00035-7.

Davis, D., Suppe, J. & Dahlen, F.A. (1983) Mechanics of Fold-and-Thrust Belts and Accretionary Wedges. *Journal of Geophysical Research: Solid Earth*, **88,** 1153-1172. doi:10.1029/JB088iB02p01153.

DeCelles, P.G., Gehrels, G.E., Quade, J. & Ojha, T.P. (1998a) Eocene-Early Miocene Foreland Basin Development and the History of Himalayan Thrusting, Western and Central Nepal. *Tectonics*, **17,** 741-765. 10.1029/98tc02598.

DeCelles, P.G., Gehrels, G.E., Quade, J., Ojha, T.P., Kapp, P.A. & Upreti, B.N. (1998b) Neogene Foreland Basin Deposits, Erosional Unroofing, and the Kinematic History of the Himalayan Fold-Thrust Belt, Western Nepal. *Geological Society of America Bulletin*, **110,** 2-21. doi:10.1130/0016-7606(1998)110<0002:NFBDEU>2.3.CO;2.

DeCelles, P.G., Gehrels, G.E., Quade, J., LaReau, B. & Spurlin, M. (2000) Tectonic Implications of U-Pb Zircon Ages of the Himalayan Orogenic Belt in Nepal. *Science*, **288,** 497-499. doi:10.1126/science.288.5465.497.

DeCelles, P.G., Gehrels, G.E., Najman, Y., Martin, A.J., Carter, A. & Garzanti, E. (2004) Detrital Geochronology and Geochemistry of Cretaceous–Early Miocene Strata of Nepal: Implications for Timing and Diachroneity of Initial Himalayan Orogenesis. *Earth and Planetary Science Letters*, **227,** 313-330. doi:10.1016/j.epsl.2004.08.019.

DeCelles, P.G., Kapp, P., Gehrels, G.E. & Ding, L. (2014) Paleocene-Eocene Foreland Basin Evolution in the Himalaya of Southern Tibet and Nepal: Implications for the Age of Initial India-Asia Collision. *Tectonics*, **33,** 824–849. doi:10.1002/ 2014TC003522.

DeCelles, P.G., Carrapa, B., Gehrels, G.E., Chakraborty, T. & Ghosh, P. (2016) Along-Strike Continuity of Structure, Stratigraphy, and Kinematic History in the Himalayan Thrust Belt: The View from Northeastern India. *Tectonics*, **35,** 2995–3027. doi:10.1002/2016TC004298.

Deeken, A., Thiede, R.C., Sobel, E.R., Hourigan, J.K. & Strecker, M.R. (2011) Exhumational Variability within the Himalaya of Northwest India. *Earth and Planetary Science Letters*, **305,** 103-114. doi:10.1016/j.epsl.2011.02.045.

Dettman, D.L., Kohn, M.J., Quade, J., Ryerson, F.J., Ojha, T.P. & Hamidullah, S. (2001) Seasonal Stable Isotope Evidence for a Strong Asian Monsoon Throughout the Past 10.7 M.Y. *Geology*, **29,** 31-34. doi:10.1130/0091-7613(2001)029<0031:SSIEFA>2.0.CO;2.

DiPietro, J.A. & Pogue, K.R. (2004) Tectonostratigraphic Subdivisions of the Himalaya: A View from the West. *Tectonics*, **23**. doi:10.1029/2003TC001554.

Eugster, P., Thiede, R.C., Scherler, D., Stübner, K., Sobel, E.R. & Strecker, M.R. (2018) Segmentation of the Main Himalayan Thrust Revealed by Low-Temperature Thermochronometry in the Western Indian Himalaya. *Tectonics*, **37,** 2710-2726. doi:10.1029/2017TC004752.

Farnsworth, A., Lunt, D.J., Robinson, S.A., Valdes, P.J., Roberts, W.H.G., Clift, P.D., Markwick, P., Su, T., Wrobel, N., Bragg, F., Kelland, S.-J. & Pancost, R.D. (2019) Past East Asian Monsoon Evolution Controlled by Paleogeography, Not Co≪Sub≫2≪/Sub&Gt. *Science Advances*, **5,** eaax1697. doi:10.1126/sciadv.aax1697.

Feakins, S.J., Liddy, H.M., Tauxe, L., Galy, V., Feng, X., Tierney, J.E., Miao, Y. & Warny, S. (2020) Miocene C4 Grassland Expansion as Recorded by the Indus Fan. *Paleoceanography and Paleoclimatology*, **35,** e2020PA003856. doi:10.1029/2020PA003856.

Fedo, C.M., Nesbitt, H.W. & Young, G.M. (1995) Unraveling the Effects of Potassium Metasomatism in Sedimentary Rocks and Paleosols, with Implications for Paleoweathering Conditions and Provenance. *Geology*, **23,** 921–924. doi:10.1130/0091-7613(1995)023<0921:UTEOPM>2.3.CO;2.

Filippelli, G.M. (1997) Intensification of the Asian Monsoon and a Chemical Weathering Event in the Late Miocene-Early Pliocene: Implications for Late Neogene Climate Change. *Geology*, **25,** 27-30. doi:10.1130/0091-7613(1997)025<0027:IOTAMA>2.3.CO;2.

France-Lanord, C., Derry, L. & Michard, A. (1993) Evolution of the Himalaya since Miocene Time: Isotopic and Sedimentologic Evidence from the Bengal Fan In: *Himalayan Tectonics* (Ed. by P. J. Treloar & M. P. Searle), *Special Publications*, **74**, 603–621. Geological Society, London.

Frank, W., Grasemann, B., Guntli, P. & Miller, C. (1995) Geological Map of the Kishtwar-Chamba-Kulu Region (Nw Himalayas, India). *Jahrbuch der Geologischen Bundesanstalt*, **138,** 299-308.

Galbraith, R.F. (1990) The Radial Plot: Graphical Assessment of Spread in Ages *Nuclear Tracks and Radiation Measurement*, **17,** 207–214. doi:10.1016/1359-0189(90)90036-W.

Garzanti, E., Baud, A. & Mascle, G. (1987) Sedimentary Record of the Northward Flight of India and Its Collision with Eurasia (Ladakh Himalaya, India). *Geodinamica Acta*, **1,** 297–312. doi:10.1080/09853111.1987.11105147.

Garzanti, E., Vezzoli, G., Ando, S., Paparella, P. & Clift, P.D. (2005) Petrology of Indus River Sands; a Key to Interpret Erosion History of the Western Himalayan Syntaxis. *Earth and Planetary Science Letters*, **229,** 287-302. doi: 10.1016/j.epsl.2004.11.008.

Garzanti, E., Liang, W., Andò, S., Clift, P.D., Resentini, A., Vermeesch, P. & Vezzoli, G. (2020) Provenance of Thal Desert Sand: Focused Erosion in the Western Himalayan Syntaxis and Foreland-Basin Deposition Driven by Latest Quaternary Climate Change. *Earth-Science Reviews*, **207,** 103220. doi:10.1016/j.earscirev.2020.103220.

Gehrels, G., Kapp, P., DeCelles, P., Pullen, A., Blakey, R., Weislogel, A., Ding, L., Guynn, J., Martin, A., McQuarrie, N. & Yin, A. (2011) Detrital Zircon Geochronology of Pre-

Tertiary Strata in the Tibetan-Himalayan Orogen. *Tectonics*, **30,** TC5016. doi:10.1029/2011tc002868.

Gehrels, G.E., DeCelles, P.G., Ojha, T.P. & Upreti, B.N. (2006) Geologic and U-Th-Pb Geochronologic Evidence for Early Paleozoic Tectonism in the Kathmandu Thrust Sheet, Central Nepal Himalaya. *Geological Society of America Bulletin*, **118,** 185-198. doi:10.1130/b25753.1.

Godard, V., Bourlès, D.L., Spinabella, F., Burbank, D.W., Bookhagen, B., Fisher, G.B., Moulin, A. & Léanni, L. (2014) Dominance of Tectonics over Climate in Himalayan Denudation. *Geology*, **42,** 243-246. doi:10.1130/g35342.1.

Green, O.R., Searle, M.P., Corfield, R.I. & Corfield, R.M. (2008) Cretaceous-Tertiary Carbonate Platform Evolution and the Age of the India-Asia Collision Along the Ladakh Himalaya (Northwest India). *Journal of Geology*, **116,** 331–353. doi: 10.1086/588831.

Gupta, A.K., Yuvaraja, A., Prakasam, M., Clemens, S.C. & Velu, A. (2015) Evolution of the South Asian Monsoon Wind System since the Late Middle Miocene. *Palaeogeography, Palaeoclimatology, Palaeoecology*, **438,** 160–167. doi:10.1016/j.palaeo.2015.08.006.

Henderson, A.L., Najman, Y., Parrish, R., BouDagher-Fadel, M., Barford, D., Garzanti, E. & Andò, S. (2010) Geology of the Cenozoic Indus Basin Sedimentary Rocks: Paleoenvironmental Interpretation of Sedimentation from the Western Himalaya During the Early Phases of India-Eurasia Collision *Tectonics*, **29**. doi:10.1029/2009TC002651.

Herron, M.M. (1988) Geochemical Classification of Terrigenous Sands and Shales from Core or Log Data. *Journal of Sedimentary Petrology*, **58,** 820–829. doi;10.1306/212F8E77-2B24-11D7-8648000102C1865D.

Horton, F. & Leech, M.L. (2013) Age and Origin of Granites in the Karakoram Shear Zone and Greater Himalaya Sequence, Nw India. *Lithosphere*, **5,** 300-320. 10.1130/l213.1.

Huang, Y., Clemens, S.C., Liu, W., Wang, Y. & Prell, W.L. (2007) Large-Scale Hydrological Change Drove the Late Miocene C4 Plant Expansion in the Himalayan Foreland and Arabian Peninsula. *Geology*, **35,** 531-534. doi:10.1130/G23666A.1.

Hughes, N.C. (2016) The Cambrian Palaeontological Record of the Indian Subcontinent. *Earth-Science Reviews*, **159,** 428-461. doi:10.1016/j.earscirev.2016.06.004.

Hurford, A. (1990) Standardization of Fission Track Dating Calibration: Recommendation by the Fission Track Working Group of the Iugs Subcommission on Geochronology. *Chemical Geology*, **80,** 177–178. doi:10.1016/0168-9622(90)90025-8.

Huyghe, P., Guilbaud, R., Bernet, M., Galy, A. & Gajurel, A.P. (2010) Significance of the Clay Mineral Distribution in Fluvial Sediments of the Neogene to Recent Himalayan Foreland Basin (West-Central Nepal). *Basin Research*, **22**. doi: 10.1111/j.1365-2117.2010.00485.x.

Huyghe, P., Bernet, M., Galy, A., Naylor, M., Cruz, J., Gyawali, B.R., Gemignani, L. & Mugnier, J.L. (2020) Rapid Exhumation since at Least 13 Ma in the Himalaya Recorded by Detrital Apatite Fission-Track Dating of Bengal Fan (Iodp Expedition 354) and Modern Himalayan River Sediments. *Earth and Planetary Science Letters*, **534,** 116078. doi:10.1016/j.epsl.2020.116078.

Johnson, D., Hooper, P. & Conrey, R. (1999) Xrf Method Xrf Analysis of Rocks and Minerals for Major and Trace Elements on a Single Low Dilution Li-Tetraborate Fused Bead. *Adv. X-ray anal*, **41,** 843-867.

Johnson, N.M., Stix, J., Tauxe, L., Cerveny, P.F. & Tahirkheli, R.A.K. (1985) Palaeomagnetic Chronology, Fluvial Processes and Tectonic Implications of the Siwalik Deposits near Chinji Village, Pakistan. *Journal of Geology*, **93,** 27–40. doi:10.1086/628917.

Jonell, T.N., Carter, A., Böning, P., Pahnke, K. & Clift, P.D. (2017) Climatic and Glacial Impact on Erosion Patterns and Sediment Provenance in the Himalayan Rain Shadow, Zanskar River, Nw India. *Geological Society of America Bulletin*, **129,** 820-836. doi:10.1130/b31573.1.

Karim, A. & Veizer, J. (2002) Water Balance of the Indus River Basin and Moisture Source in the Karakoram and Western Himalayas: Implications from Hydrogen and Oxygen Isotopes River Water. *Journal of Geophysical Research*, **107**. doi:10.1029/2000JD000253.

Kohn, M.J., Paul, S.K. & Corrie, S.L. (2009) The Lower Lesser Himalayan Sequence: A Paleoproterozoic Arc on the Northern Margin of the Indian Plate. *Geological Society of America Bulletin*, **122,** 323-335. doi:10.1130/b26587.1.

Kroon, D., Steens, T. & Troelstra, S.R. (1991) Onset of Monsoonal Related Upwelling in the Western Arabian Sea as Revealed by Planktonic Foraminifers. In: *Proceedings of the Ocean Drilling Program, Scientific Results* (Ed. by W. Prell & N. Niitsuma), **117**, 257–263. Ocean Drilling Program, College Station, TX.

Lavé, J. & Avouac, J.P. (2000) Active Folding of Fluvial Terraces across the Siwaliks Hills (Himalayas of Central Nepal). *Journal of Geophysical Research*, **105,** 5735–5770. doi: 10.1029/1999JB900292.

Li, Y., Clift, P.D., Böning, P., Blusztajn, J., Murray, R.W., Ireland, T., Pahnke, K., Helm, N.C. & Giosan, L. (2018) Continuous Holocene Input of River Sediment to the Indus Submarine Canyon. *Marine Geology*, **406,** 159-176. doi:10.1016/j.margeo.2018.09.011.

Mandal, S.K., Scherler, D., Romer, R.L., Burg, J.-P., Guillong, M. & Schleicher, A.M. (2019) Multiproxy Isotopic and Geochemical Analysis of the Siwalik Sediments in Nw India: Implication for the Late Cenozoic Tectonic Evolution of the Himalaya. *Tectonics,* **38,** 120-143. doi:10.1029/2018TC005200.

Martin, A.J., DeCelles, P.G., Gehrels, G.E., Patchett, P.J. & Isachsen, C. (2005) Isotopic and Structural Constraints on the Location of the Main Central Thrust in the Annapurna Range, Central Nepal Himalaya. *Geological Society of America Bulletin*, **117**. doi:10.1130/b25646.1.

Martin, A.J., Ganguly, J. & DeCelles, P.G. (2009) Metamorphism of Greater and Lesser Himalayan Rocks Exposed in the Modi Khola Valley, Central Nepal. *Contributions to Mineralogy and Petrology*, **159,** 203-223. doi:10.1007/s00410-009-0424-3.

McKenzie, N.R., Hughes, N.C., Myrow, P.M., Xiao, S. & Sharma, M. (2011) Correlation of Precambrian–Cambrian Sedimentary Successions across Northern India and the Utility of Isotopic Signatures of Himalayan Lithotectonic Zones. *Earth and Planetary Science Letters*, **312,** 471-483. doi:10.1016/j.epsl.2011.10.027.

McLennan, S., Hemming, S., McDaniel, D. & Hanson, G. (1993) Geochemical Approaches to Sedimentation, Provenance, and Tectonics (Ed. by M. J. Johnson & A. Basu), *Special Papers*, **284**, 21-21. Geological Society of America, Boulder. doi:10.1130/SPE284-p21.

McNeill, L.C., Dugan, B., Backman, J., Pickering, K.T., Pouderoux, H.F.A., Henstock, T.J., Petronotis, K.E., Carter, A., Chemale, F., Milliken, K.L., Kutterolf, S., Mukoyoshi, H., Chen, W., Kachovich, S., Mitchison, F.L., Bourlange, S., Colson, T.A., Frederik, M.C.G., Guèrin, G., Hamahashi, M., House, B.M., Hüpers, A., Jeppson, T.N., Kenigsberg, A.R., Kuranaga, M., Nair, N., Owari, S., Shan, Y., Song, I., Torres, M.E., Vannucchi, P., Vrolijk, P.J., Yang, T., Zhao, X. & Thomas, E. (2017) Understanding Himalayan Erosion and the Significance of the Nicobar Fan. *Earth and Planetary Science Letters*, **475,** 134-142. doi:10.1016/j.epsl.2017.07.019.

McQuarrie, N., Robinson, D., Long, S., Tobgay, T., Grujic, D., Gehrels, G. & Ducea, M. (2008) Preliminary Stratigraphic and Structural Architecture of Bhutan: Implications for the Along Strike Architecture of the Himalayan System. *Earth and Planetary Science Letters*, **272,** 105-117. doi:10.1016/j.epsl.2008.04.030.

Meigs, A.J., Burbank, D.W. & Beck, R.A. (1995) Middle-Late Miocene (>10 Ma) Formation of the Main Boundary Thrust in the Western Himalaya. *Geology*, **23,** 423-426. doi:10.1130/0091-7613(1995)023<0423:MLMMFO>2.3.CO;2.

Miller, C., Klötzli, U., Frank, W., Thöni, M. & Grasemann, B. (2000) Proterozoic Crustal Evolution in the Nw Himalaya (India) as Recorded by Circa 1.80 Ga Mafic and 1.84 Ga Granitic Magmatism. *Precambrian Research*, **103,** 191-206. doi:10.1016/S0301-9268(00)00091-7.

Miller, C., Thöni, M., Frank, W., Grasemann, B., Klötzli, U., Guntli, P. & Draganits, E. (2001) The Early Palaeozoic Magmatic Event in the Northwest Himalaya, India: Source, Tectonic Setting and Age of Emplacement. *Geological Magazine*, **138,** 237-251. doi:10.1017/s0016756801005283.

Molnar, P., England, P. & Martinod, J. (1993) Mantle Dynamics, Uplift of the Tibetan Plateau, and the Indian Monsoon. *Reviews of Geophysics*, **31,** 357-396. doi:10.1029/93RG02030.

Molnar, P. & Stock, J.M. (2009) Slowing of India's Convergence with Eurasia since 20 Ma and Its Implications for Tibetan Mantle Dynamics. *Tectonics*, **28**. doi:10.1029/2008TC002271.

Murphy, M.A. & Yin, A. (2003) Structural Evolution and Sequence of Thrusting in the Tethyan Fold-Thrust Belt and Indus-Yalu Suture Zone, Southwest Tibet. *GSA Bulletin*, **115,** 21-34. doi:10.1130/0016-7606(2003)115<0021:Seasot>2.0.Co;2.

Myrow, P.M., Hughes, N.C., Paulsen, T.S., Williams, I.S., Parcha, S.K., Thompson, K.R., Bowring, S.A., Peng, S.C. & Ahluwalia, A.D. (2003) Integrated Tectonostratigraphic Analysis of the Himalaya and Implications for Its Tectonic Reconstruction. *Earth and Planetary Science Letters*, **212,** 433-441. doi:10.1016/s0012-821x(03)00280-2.

Myrow, P.M., Hughes, N.C., Goodge, J.W., Fanning, C.M., Williams, I.S., Peng, S., Bhargava, O.N., Parcha, S.K. & Pogue, K.R. (2010) Extraordinary Transport and Mixing of Sediment across Himalayan Central Gondwana During the Cambrian-Ordovician. *Geological Society of America Bulletin*, **122,** 1660-1670. doi:10.1130/b30123.1.

Myrow, P.M., Hughes, N.C., Derry, L.A., McKenzie, R.N., Jiang, G., Webb, A.A.G., Banerjee, D.M., Paulsen, T.S. & Singh, B.P. (2015) Neogene Marine Isotopic Evolution and the Erosion of Lesser Himalayan Strata: Implications for Cenozoic Tectonic History. *Earth and Planetary Science Letters*, **417,** 142-150. doi:10.1016/j.epsl.2015.02.016.

Najman, Y., Johnson, K., White, N. & Oliver, G. (2004) Evolution of the Himalayan Foreland Basin, Nw India. *Basin Research*, **16,** 1-24. doi:10.1111/j.1365-2117.2004.00223.x.

Najman, Y. (2006) The Detrital Record of Orogenesis: A Review of Approaches and Techniques Used in the Himalayan Sedimentary Basins. *Earth-Science Reviews*, **74,** 1 –72. 10.1016/j.earscirev.2005.04.004.

Najman, Y., Bickle, M., Garzanti, E., Pringle, M., Barfod, D., Brozovic, N., Burbank, D. & Ando, S. (2009) Reconstructing the Exhumation History of the Lesser Himalaya, Nw India, from a Multitechnique Provenance Study of the Foreland Basin Siwalik Group. *Tectonics*, **28,** n/a-n/a. doi:10.1029/2009tc002506.

Najman, Y., Bickle, M., Garzanti, E., Pringle, M., Barfod, D., Brozovic, N., Burbank, D. & Ando, S. (2010) Correction to “Reconstructing the Exhumation History of the Lesser

Himalaya, Nw India, from a Multitechnique Provenance Study of the Foreland Basin Siwalik Group". *Tectonics*, **29**. doi:10.1029/2010TC002778.

Najman, Y., Jenks, D., Godin, L., Boudagher-Fadel, M., Millar, I., Garzanti, E., Horstwood, M. & Bracciali, L. (2017) The Tethyan Himalayan Detrital Record Shows That India–Asia Terminal Collision Occurred by 54 Ma in the Western Himalaya. *Earth and Planetary Science Letters*, **459,** 301-310. doi:10.1016/j.epsl.2016.11.036.

Nesbitt, H.W., Markovics, G. & Price, R.C. (1980) Chemical Processes Affecting Alkalis and Alkaline Earths During Continental Weathering. *Geochimica et Cosmochimica Acta*, **44,** 1659–1666. doi:10.1016/0016-7037(80)90218-5.

Parkash, B., Sharma, R.P. & Roy, A.K. (1980) The Siwalik Group (Molasses)–Sediments Shed by Collision of Continental Plates. *Sedimentary Geology*, **25,** 127–159. doi:10.1016/0037-0738(80)90058-5.

Parrish, R.R. & Hodges, V. (1996) Isotopic Constraints on the Age and Provenance of the Lesser and Greater Himalayan Sequences, Nepalese Himalaya. *Geological Society of America Bulletin*, **108,** 904-911. doi:10.1130/0016-7606(1996)108<0904:Icotaa>2.3.Co;2.

Prell, W.L. & Kutzbach, J.E. (1992) Sensitivity of the Indian Monsoon to Forcing Parameters and Implications for Its Evolution. *Nature*, **360,** 647-652. doi:10.1038/360647a0.

Prell, W.L., Murray, D.W., Clemens, S.C. & Anderson, D.M. (1992) Evolution and Variability of the Indian Ocean Summer Monsoon: Evidence from the Western Arabian Sea Drilling Program. In: *Synthesis of Results from Scientific Drilling in the Indian Ocean* (Ed. by R. A. Duncan, D. K. Rea, R. B. Kidd, U. von Rad & J. K. Weissel), *Geophysical Monograph*, **70**, 447–469. American Geophysical Union, Washington, DC.

Quade, J., Cerling, T.E. & Bowman, J.R. (1989) Development of Asian Monsoon Revealed by Marked Ecological Shift During the Latest Miocene in Northern Pakistan. *Nature*, **342,** 163-166. doi:10.1038/342163a0.

Ravikant, V., Wu, F.-Y. & Ji, W.-Q. (2011) U–Pb Age and Hf Isotopic Constraints of Detrital Zircons from the Himalayan Foreland Subathu Sub-Basin on the Tertiary Palaeogeography of the Himalaya. *Earth and Planetary Science Letters*, **304,** 356-368. doi:10.1016/j.epsl.2011.02.009.

Richards, A., Argels, T., Harris, N., Parrish, R., Ahmad, T., Darbyshire, F. & Dragantis, E. (2005) Himalayan Architecture Constrained by Isotopic Tracers from Clastic Sediments. *Earth and Planetary Science Letters*, **236,** 773-796. doi:10.1016/j.epsl.2005.05.034.

Robert, X., van der Beek, P., Braun, J., Perry, C. & Mugnier, J.-L. (2011) Control of Detachment Geometry on Lateral Variations in Exhumation Rates in the Himalaya: Insights from Low-Temperature Thermochronology and Numerical Modeling. *Journal of Geophysical Research: Solid Earth*, **116**. doi:10.1029/2010JB007893.

Robinson, D.M., DeCelles, P.G., Patchett, P.J. & Garzione, C.N. (2001) The Kinematic Evolution of the Nepalese Himalaya Interpreted from Nd Isotopes. *Earth and Planetary Science Letters*, **192,** 507-521. doi:10.1016/S0012-821X(01)00451-4.

Robinson, D.M., DeCelles, P.G. & Copeland, P. (2006) Tectonic Evolution of the Himalayan Thrust Belt in Western Nepal; Implications for Channel Flow Models. *Geological Society of America Bulletin*, **118,** 865-885. doI;10.1130/B25911.1.

Sahni, A. & Srivastava, V.C. (1976) Eocene Rodents and Associated Reptiles from the Subathu Formation of Northwestern India. *Journal of Paleontology*, **50,** 922-928.

Schlup, M., Steck, A., Carter, A., Cosca, M., Epard, J.-L. & Hunziker, J. (2011) Exhumation History of the Nw Indian Himalaya Revealed by Fission Track and 40ar/39ar Ages. *Journal of Asian Earth Sciences*, **40,** 334-350. doi:10.1016/j.jseaes.2010.06.008.

Schwertmann, U. (1971) Transformation of Hematite to Goethite in Soils. *Nature*, **232,** 624–625.

Singh, P. (2009) Major, Trace and Ree Geochemistry of the Ganga River Sediments: Influence of Provenance and Sedimentary Processes. *Chemical Geology*, **266,** 242-255. doi:10.1016/j.chemgeo.2009.06.013.

Singh, S., Parkash, B., Awasthi, A.K. & Kumar, S. (2011) Late Miocene Record of Palaeovegetation from Siwalik Palaeosols of the Ramnagar Sub-Basin, India. *Current Science*, **100,** 213-222.

Singh, T., Awasthi, A.K. & Caputo, R. (2012) The Sub-Himalayan Fold-Thrust Belt in the 1905 Kangra Earthquake Zone: A Critical Taper Model Perspective for Seismic Hazard Analysis. *Tectonics*, **31**. doi:10.1029/2012TC003120.

Sorkhabi, R.B. & Arita, K. (1997) Toward a Solution for the Himalayan Puzzle: Mechanism of Inverted Metamorphism Constrained by the Siwalik Sedimentary Record. *Current Science*, **72,** 862-873.

Steck, A. (2003) Geology of the Nw Indian Himalaya. *Eclogae Geol Helv*, **96,** 147-196.

Stevens, V.L. & Avouac, J.P. (2015) Interseismic Coupling on the Main Himalayan Thrust. *Geophysical Research Letters*, **42,** 5828-5837. doi:10.1002/2015GL064845.

Stübner, K., Grujic, D., Dunkl, I., Thiede, R. & Eugster, P. (2018) Pliocene Episodic Exhumation and the Significance of the Munsiari Thrust in the Northwestern Himalaya. *Earth and Planetary Science Letters*, **481,** 273-283. doi:10.1016/j.epsl.2017.10.036.

Sundell, K. & Saylor, J.E. (2017) Unmixing Detrital Geochronology Age Distributions. *Geochemistry Geophysics Geosystems*, **18,** 2872–2886. doi:10.1002/2016GC006774.

Tewari, V. (2003) Sedimentology, Palaeobiology and Stable Isotope Chemostratigraphy of the Terminal Neoproterozoic Buxa Dolomite, Arunachal Pradesh, Ne Lesser Himalaya. *Journal of Himalayan Geology*, **18,** 1–18.

Thakur, S.S. & Tripathi, K. (2008) Regional Metamorphism in the Haimanta Group of Rocks, Sutlej River Valley, Nw Himalaya, India. *Current Science*, **95,** 104-109.

Thakur, V.C., Jayangondaperumal, R. & Malik, M.A. (2010) Redefining Medlicott–Wadia's Main Boundary Fault from Jhelum to Yamuna: An Active Fault Strand of the Main Boundary Thrust in Northwest Himalaya. *Tectonophysics*, **489,** 29-42. doi:10.1016/j.tecto.2010.03.014.

Thiede, R., Robert, X., Stübner, K., Dey, S. & Faruhn, J. (2017) Sustained out-of-Sequence Shortening Along a Tectonically Active Segment of the Main Boundary Thrust: The Dhauladhar Range in the Northwestern Himalaya. *Lithosphere*, **9,** 715-725. doi:10.1130/l630.1.

Thiede, R.C., Bookhagen, B., Arrowsmith, J.R., Sobel, E.R. & Strecker, M.R. (2004) Climatic Control on Rapid Exhumation Along the Southern Himalayan Front. *Earth and Planetary Science Letters*, **222,** 791-806. doi:10.1016/j.epsl.2004.03.015.

Thiede, R.C., Ehlers, T.A., Bookhagen, B. & Strecker, M.R. (2009) Erosional Variability Along the Northwest Himalaya. *Journal of Geophysical Research*, **114**. doi:10.1029/2008JF001010.

Thiede, R.C. & Ehlers, T.A. (2013) Large Spatial and Temporal Variations in Himalayan Denudation. *Earth and Planetary Science Letters*, **374,** 256-257. doi:10.1016/j.epsl.2013.03.004.

Valdiya, K. (1980) Geology of Kumaun Lesser Himalaya, Wadia Institute of Himalayan Geology. Dehradun, India**,** 1-291.

van der Beek, P., Robert, X., Mugnier, J.-L., Bernet, M., Huyghe, P. & Labrin, E. (2006) Late Miocene-Recent Exhumation of the Central Himalaya and Recycling in the Foreland

Basin Assessed by Apatite Fission-Track Thermochronology of Siwalik Sediments, Nepal. *Basin Research*, **18,** 413-434. doi:10.1111/j.1365-2117.2006.00305.x.

van Hinsbergen, D.J.J., Lippert, P.C., Dupont-Nivet, G., McQuarrie, N., Doubrovine, P.V., Spakman, W. & Torsvik, T.H. (2012) Greater India Basin Hypothesis and a Two-Stage Cenozoic Collision between India and Asia. *Proceedings Of The National Academy of Sciences*, **109,** 7659-7664. doi:10.1073/pnas.1117262109.

Vannay, J. & Grasemann, B. (1998) Inverted Metamorphism in the High Himalaya of Himachal Pradesh (Nw India): Phase Equilibria Versus Thermobarometry. *Schweizerische Mineralogische und Petrographische Mitteilungen*, **78,** 107-132.

Vannay, J.-C., Grasemann, B., Rahn, M., Frank, W., Carter, A., Baudraz, V. & Cosca, M. (2004) Miocene to Holocene Exhumation of Metamorphic Crustal Wedges in the Nw Himalaya: Evidence for Tectonic Extrusion Coupled to Fluvial Erosion. *Tectonics*, **23**. doi:10.1029/2002TC001429.

Vermeesch, P. (2013) Multi-Sample Comparison of Detrital Age Distributions. *Chemical Geology*, **341,** 140–146. doi:10.1016/j.chemgeo.2013.01.010.

Vögeli, N., Najman, Y., van der Beek, P., Huyghe, P., Wynn, P.M., Govin, G., Veen, I.v.d. & Sachse, D. (2017a) Lateral Variations in Vegetation in the Himalaya since the Miocene and Implications for Climate Evolution. *Earth and Planetary Science Letters*, **471,** 1–9. doi:10.1016/j.epsl.2017.04.037.

Vögeli, N., van der Beek, P., Huyghe, P. & Najman, Y. (2017b) Weathering in the Himalaya, an East-West Comparison: Indications from Major Elements and Clay Mineralogy. *The Journal of Geology*, **125,** 515–529. doi: 10.1086/692652.

Webb, A.A.G. (2013) Preliminary Palinspastic Reconstruction of Cenozoic Deformation across the Himachal Himalaya (Northwestern India). *Geosphere*, **9,** 572-587. doi:10.1130/GES00787.1.

West, A.J., Galy, A. & Bickle, M.J. (2005) Tectonic and Climatic Controls on Silicate Weathering. *Earth and Planetary Science Letters*, **235,** 211–228. doi: 10.1016/j.epsl.2005.03.020.

White, N.M., Parrish, R.R., Bickle, M.J., najman, Y.M.R., Burbank, D.W. & Maithani, A. (2001) Metamorphism and Exhumation of the Nw Himalaya Constrained by U-Th-Pb Analysis of Detrital Monazite Grains from Early Foreland Basin. *Journal of the Geological Society*, **158,** 625-635. doi:10.1144/jgs.158.4.625.

White, N.M., Pringle, M., Garzanti, E., Bickle, M., Najman, Y., Chapman, H. & Friend, P. (2002) Constraints on the Exhumation and Erosion of the High Himalayan Slab, Nw India, from Foreland Basin Deposits. *Earth and Planetary Science Letters*, **195,** 29-44. doi:10.1016/s0012-821x(01)00565-9.

Willett, S.D., Fisher, D., Fuller, C., Yeh, E.-C. & Lu, C.-Y. (2003) Erosion Rates and Orogenic-Wedge Kinematics in Taiwan Inferred from Fission-Track Thermochronometry. *Geology*, **31,** 945-948. doi:10.1130/g19702.1.

Wobus, C.W., Hodges, K.V. & Whipple, K.X. (2003) Has Focused Denudation Sustained Active Thrusting at the Himalayan Topographic Front? *Geology*, **31,** 861-864.

Wu, F.Y., Ji, W.Q., Wang, J.G., Liu, C.Z., Chung, S.L. & Clift, P.D. (2014) Zircon U-Pb and Hf Isotopic Constraints on the Onset Time of India-Asia Collision. *American Journal of Science*, **314,** 548 –579. doi:10.2475/02.2014.04].

Yin, A. (2006) Cenozoic Tectonic Evolution of the Himalayan Orogen as Constrained by Along-Strike Variation of Structural Geometry, Exhumation History, and Foreland Sedimentation. *Earth-Science Reviews*, **76,** 1-131. doi:10.1016/j.earscirev.2005.05.004.

ZHOU, P., CARTER, A., LI, Y. & CLIFT, P.D. (2020) Slowing Rates of Regional Exhumation in the Western Himalaya: Fission Track Evidence from the Indus Fan. *Geological Magazine*, **157,** 848-863. doi:10.1017/S0016756819000608.

ZHOU, P., IRELAND, T., MURRAY, R.W. & CLIFT, P.D. (2021) Marine Sedimentary Records of Chemical Weathering Evolution in the Western Himalaya since 17 Ma. *Geosphere*, **17**. doi:10.1130/GES02211.1.

Figure and Table Captions

Figure 1. Geological map of the Western Himalayas showing the major tectonic units that are eroded by the Indus River and its tributaries. Map is modified after Alizai *et al.* (2011). Rivers are shown in thick black lines. ISZ – Indus Suture Zone, MCT – Main Central Thrust, MBT – Main Boundary Thrust and MFT – Main Frontal Thrust. Sample locations are shown as filled red dots. JW – Jawalamukhi and JN – Joginder Nagar.

Figure 2. (A) Topographic map of the Northwestern Himalayas made with ArcGIS Software from NASA's Shuttle Radar Topography Mission (SRTM). Red boxes show the location of the detailed study areas. Map also shows the primary source ranges, major fault systems, and reentrant zones after Singh et al. (2012). Palampur Thrust is from Thakur *et al.* (2010). ILH – Inner Lesser Himalayas, OLH – Outer Lesser Himalayas, GHS – Greater Himalayas, THS – Tethyan Himalayas, SH – Sub-Himalayas, MCT – Main Central Thrust, MBT – Main Boundary Thrust and MFT – Main Frontal Thrust, and TZ – Transition Zone. The TZ marks the transition between the Kangra and Nahan Salient Reentrants. **(B)** Sample locations for the Jawalamukhi section and **(C)** from the Joginder Nagar section on shaded SRTM topography plotted with GeoMapApp within the Kangra Reentrant.

Figure 3. Stratigraphic columns of the two foreland basin sections discussed in the text. The stratigraphic columns show thickness, lithology, and depositional ages for the Joginder Nagar (left) and the Jawalamukhi (right) sections. The depositional ages are derived from magnetostratigraphy (Meigs *et al.*, 1995). The Joginder Nagar section is modified from White *et al*. (2002) and the Jawalamukhi section is modified from Najman *et al*. (2009). Note the significant coarsening up in the Jawalamukhi section after 9 Ma.

Figure 4. (A) Geochemical signature of the analyzed samples (green symbols) illustrated by a $CaO+Na_2O-Al_2O_3-K_2O$ (CN-A-K) ternary diagram (Fedo *et al.*, 1995), together with data from Vögeli *et al.* (2017b)(orange symbols) from the same section. CaO* represents the CaO associated with silicate, excluding all the carbonate. Samples closer to Al_2O_3 are rich in kaolinite, chlorite and/or gibbsite (representing by kao, chl and gib). CIA values are also calculated and shown on the left side, with its values are correlated with the CN-A-K. Abbreviations: sm (smectite), pl (plagioclase), ksp (K-feldspar), il (illite), m (muscovite). Quaternary Indus delta are from Clift *et al.* (2010), Holocene Indus Canyon data are from Li *et al.* (2018). Neogene Indus shelf and fan data are from Zhou *et al*. (2021). B) Geochemical classification of sediments from this study following the scheme of Herron (1988).

Figure 5. Kernel density estimate (KDE) plots for the zircon U–Pb ages from the foreland sections compared with some of the major source terrains and modern Indus River tributaries, as well the Yamuna in the Western Himalayas. Bedrock compilation is from Alizai *et al*. (2011), Cawood *et al*. (2007), DeCelles *et al*. (2004), Gehrels *et al.* (2011), Horton *et al*. (2013), Jonell *et al*. (2017), Kohn *et al*. (2009), McKenzie *et al*. (2011), Myrow *et al*. (2010), Martin *et al.* (2005; 2009), McQuarrie *et al*. (2008), Miller *et al*. (2001), Parrish *et al*. (1996). Major Indus River tributaries compilation is from Alizai *et al.* (2011). Colored strips highlight provenance diagnostic age populations: Purple – 400–750 Ma, Blue – 750–900 Ma, Green – 900–1250 Ma, Brown – 1700–2000 Ma.

Figure 6. A) Multi-dimensional scalar (MDS) plot comparing the detrital samples from the Jawalamukhi and Joginder Nagar sections (yellow dots) with potential bedrock sources (red dots)

and major Indus River tributaries (blue dots). ILH – Inner Lesser Himalayas, OLH – Outer Lesser Himalayas, GHS – Greater Himalayas, and THS – Tethyan Himalayas. Data sources are as for Figure 4. Note the progressive migration away from the OLH, THS, and GHS sources and towards the ILH source starting at the 7–8 Ma sample. B) Shows the same dataset without the extreme Indus and ILH outliers.

Figure 7. Lag time plot of detrital apatite fission track central ages showing the lag time between the cooling and depositional ages. Siwalik data from Karnali, Surai Khola and Tinau Khola (Nepal) are from van der Beek *et al.* (2006), Bengal Fan data is from Corrigan & Crowley (1990). Gray shaded area shows the range of time in this study area for which the samples are clearly reset for AFT. Samples from this study are all within error of the zero lag time line.

Figure 8. Calculated contributions from bedrock source terrains to sediments considered in this study through time based on the Kuiper unmixing calculations, compared with Nd isotope data from the same section from Najman et al. (2009) showing sediment matrix and conglomerate pebbles. Carbon isotopes from paleosols constrain vegetation and are from NW India (Vögeli *et al.*, 2017a) and the Potwar Plateau, Pakistan (Quade *et al.*, 1989). Hematite data from the Arabian Sea are from Zhou *et al*. (2021).

Figure 9. Kernel density estimate (KDE) plots for the zircon U–Pb ages from the foreland sections at Dehra Dun (Mandal *et al.*, 2019) and Jawalamukhi (this study) showing the relative loss of grains 400–1250 Ma after 8 Ma at the latter site while they continue to be an important component at the former.

Figure 10. Summary figure showing the evolving drainage exposure and migration of the two foreland sections towards the range front since 20 Ma with estimated outcrop patterns based on this and earlier studies showing the passage of the sections through different river flood plains through time. Modern map is based on DiPietro & Pogue (2004). UKW = Uttarkashi Window. Location of rivers is schematic and based on the provenance of the sediment constrained in this study.

Table 1. Locations of samples and estimated depositional ages based on magnetostratigraphy. Convergence rates are from Clark (2012).

Table 2. Major and select trace element geochemical analysis of the samples considered in this study. Major element concentrations are in weight percent. Trace elements are shown as parts per million (ppm).

Table 3. Fission track analytical data

(i). Track densities are ($x10^6$ tr cm^{-2}) numbers of tracks counted (N) shown in brackets;

(ii). analyses by external detector method using 0.5 for the $4\pi/2\pi$ geometry correction factor;

(iii). ages calculated using dosimeter glass CN-5; (apatite) $\zeta CN5 = 339 \pm 5$;

calibrated by multiple analyses of IUGS apatite and zircon age standards (Hurford, 1990);

(iv). $P\chi 2$ is probability for obtaining $\chi 2$ value for v degrees of freedom, where v = no. crystals - 1;

(v). Central age is a modal age, weighted for different precisions of individual crystals (Galbraith, 1990).

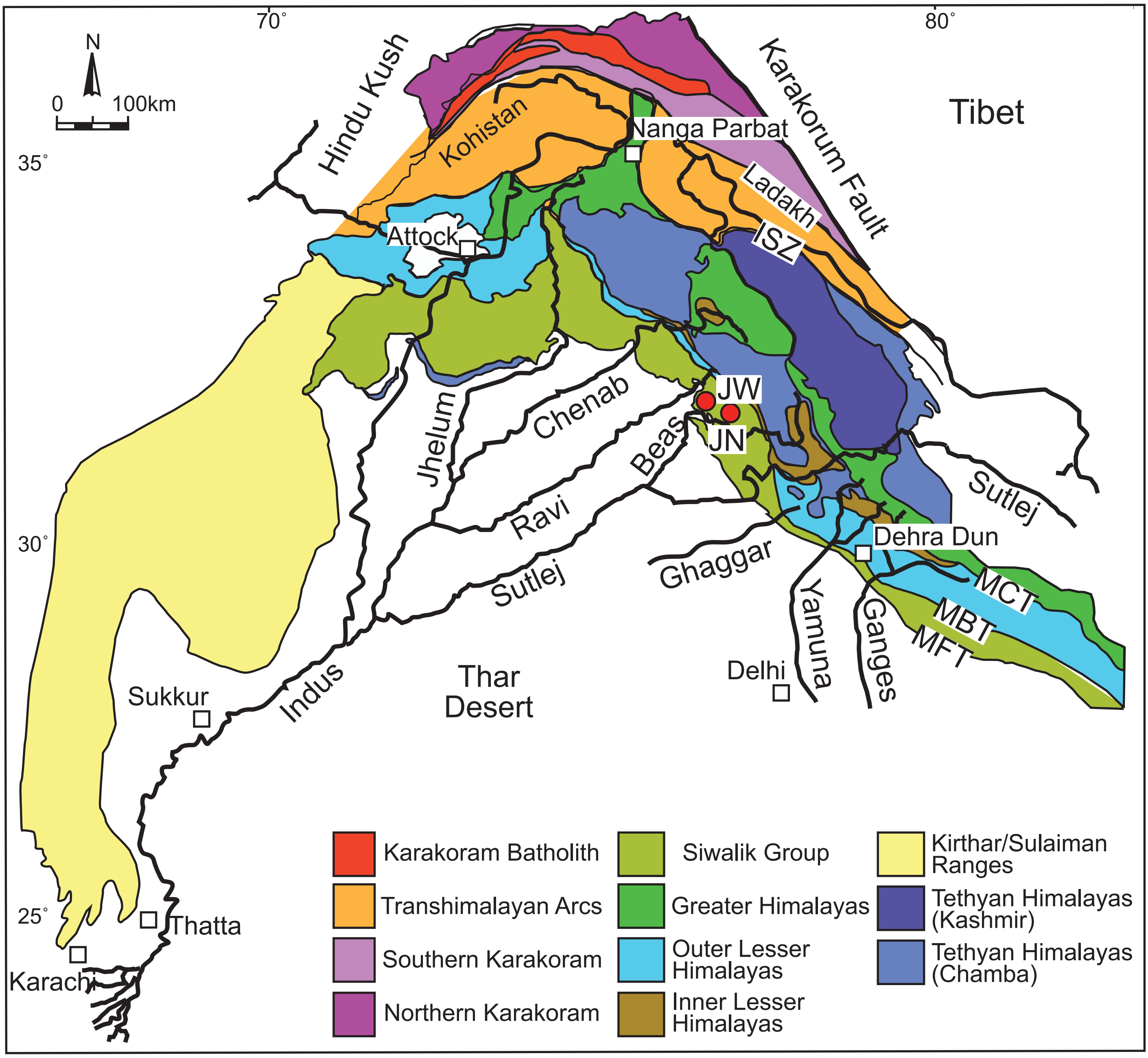

Figure 1
Exnicios et al.

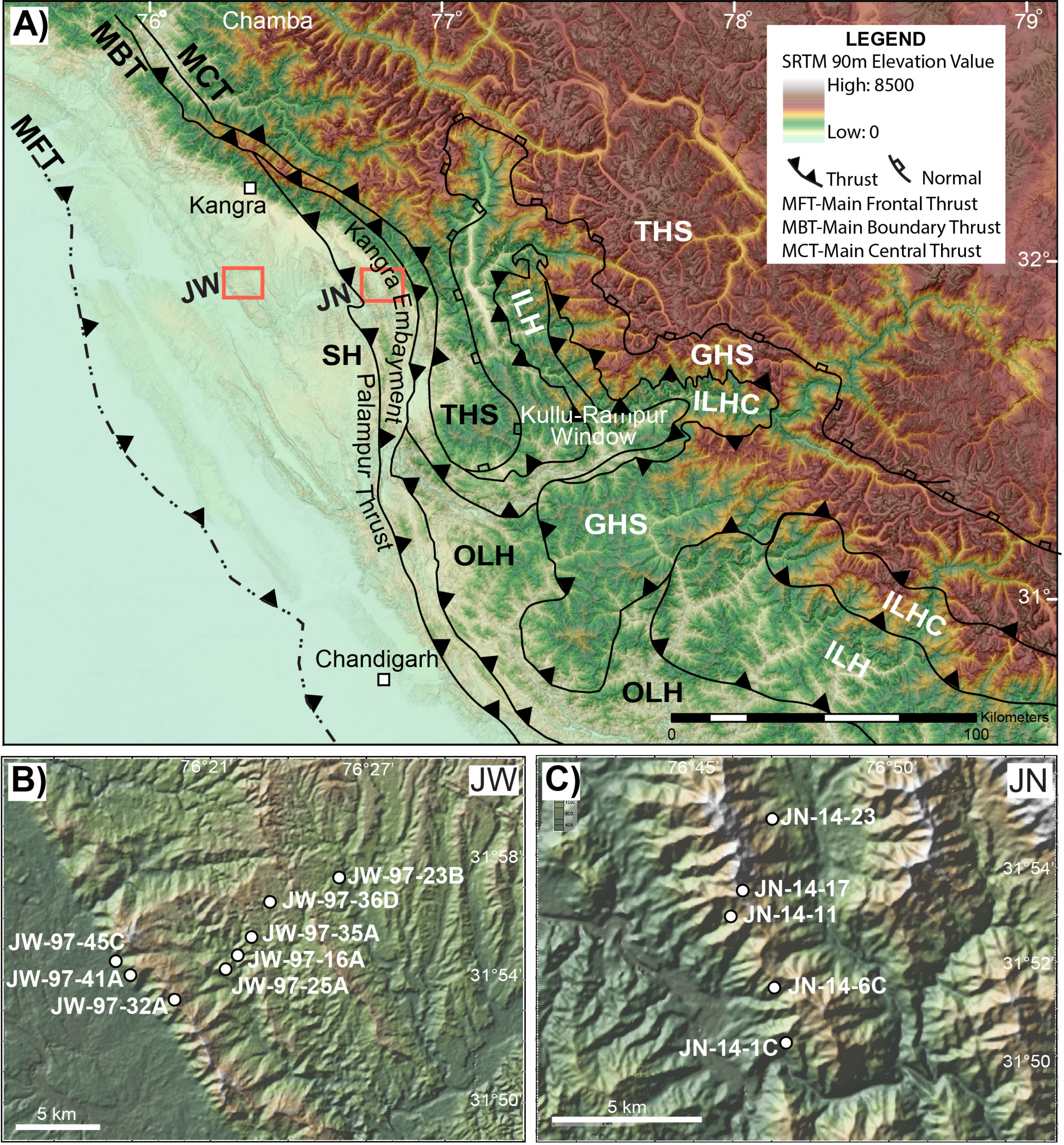

Figure 2
Exnicios et al.

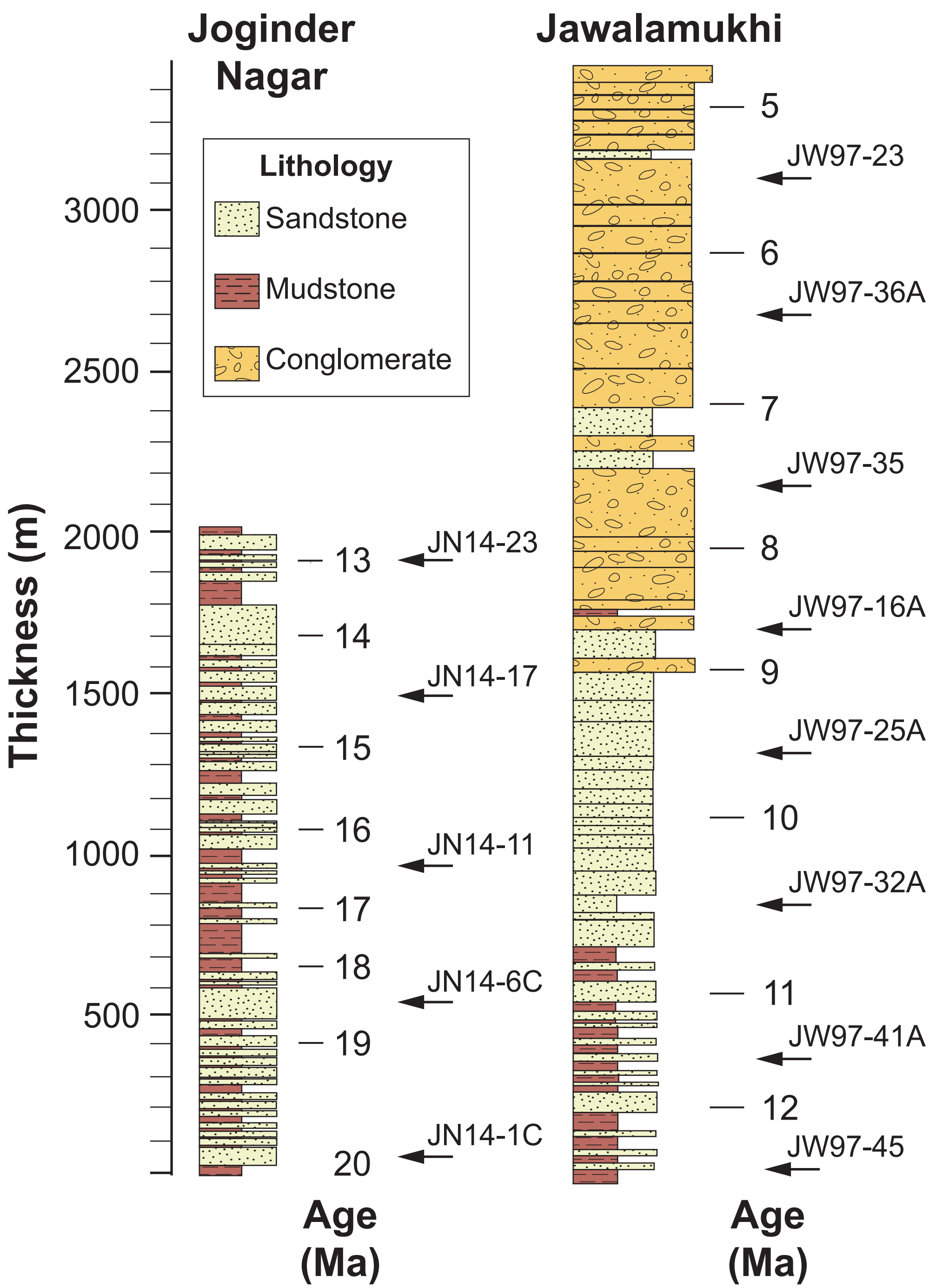

Figure 3
Exnicios et al.

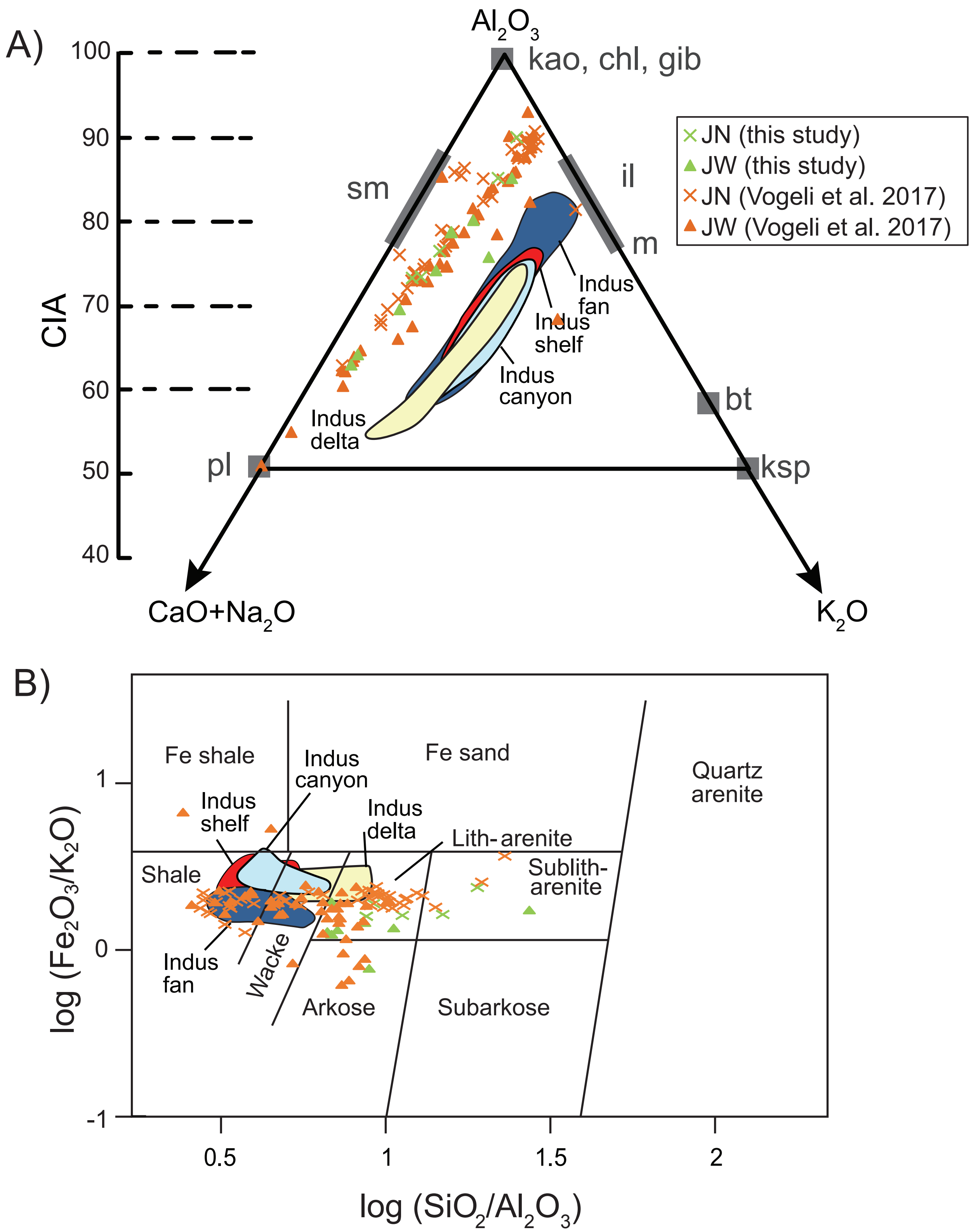

Figure 4
Exnicios et al.

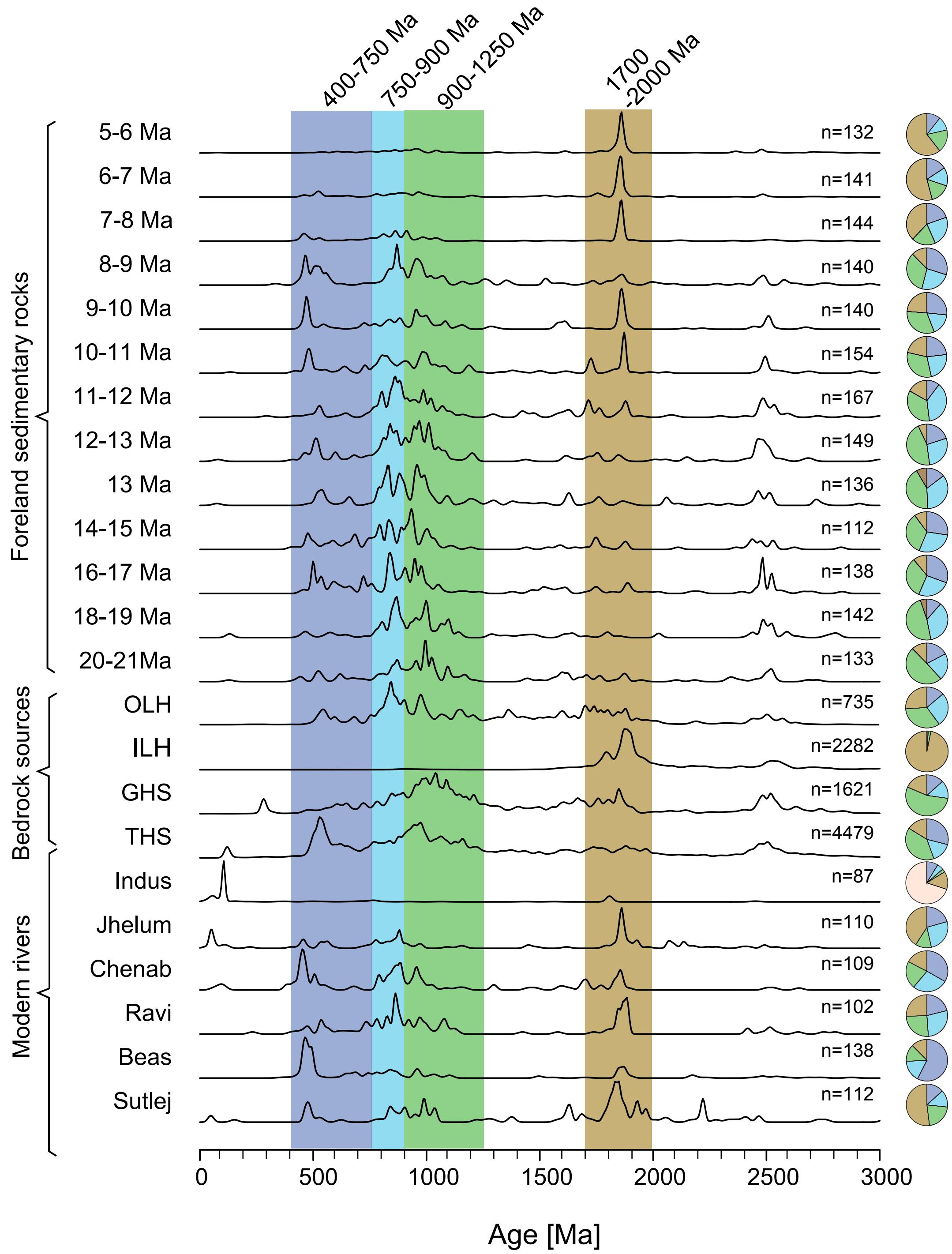

Figure 5
Exnicios et al.

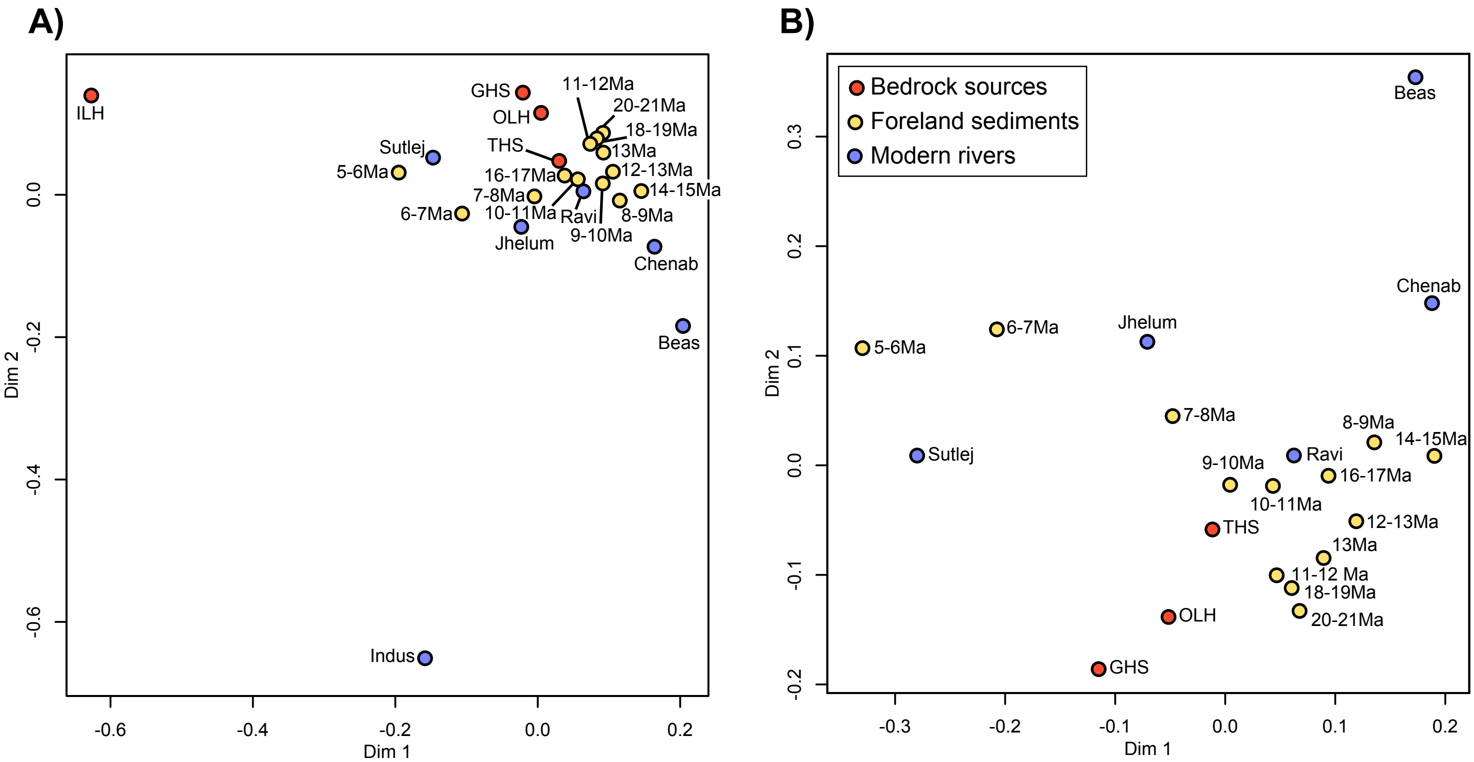

Figure 6
Exnicios et al.

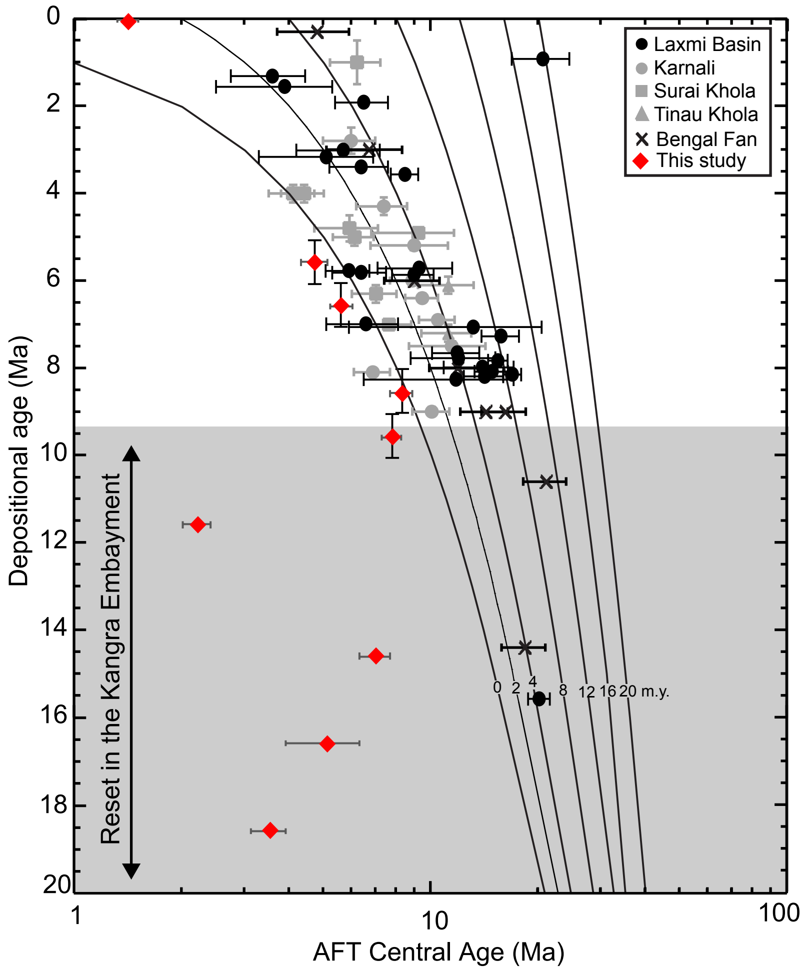

Figure 7
Exnicios et al.

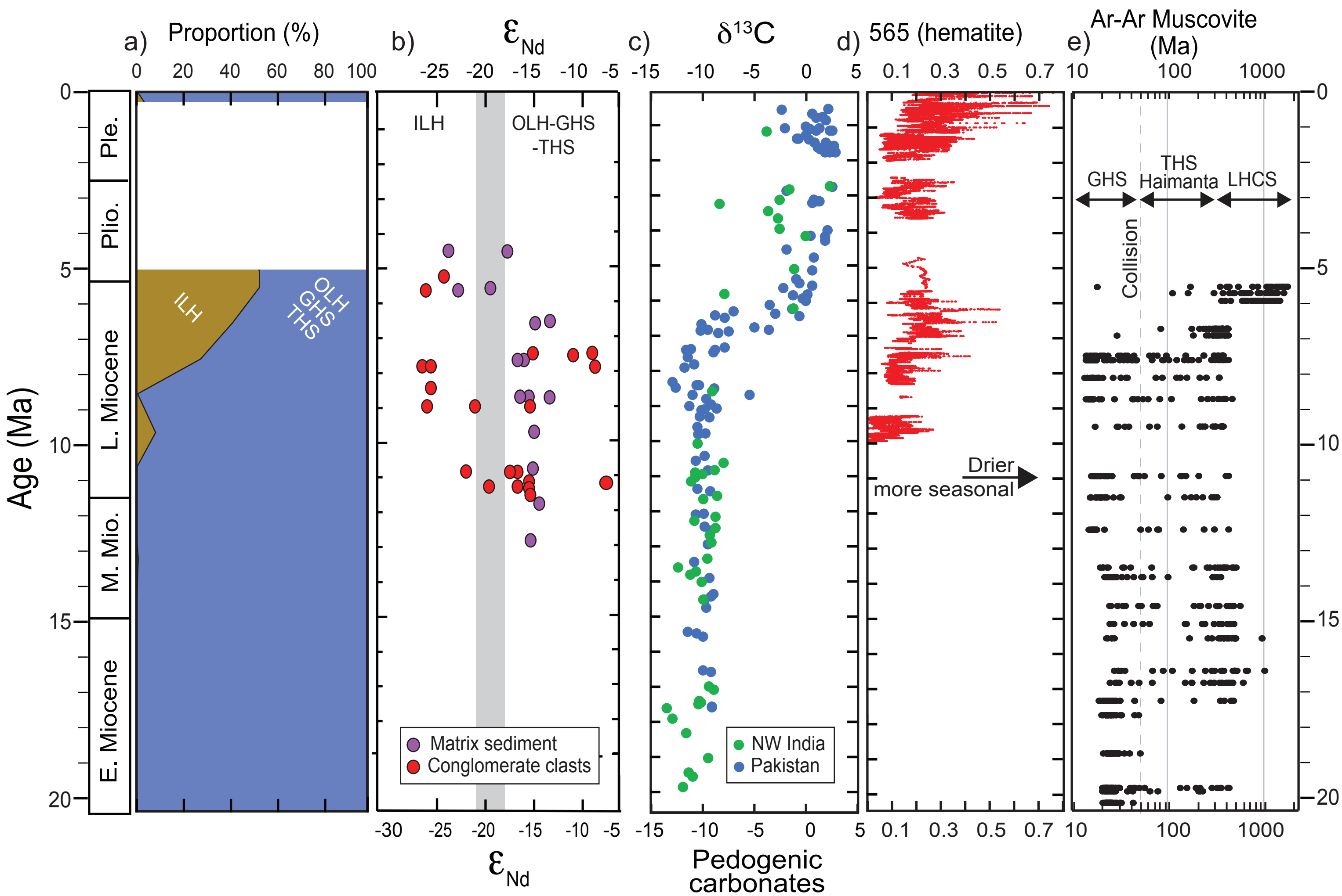

Figure 8
Exnicios et al.

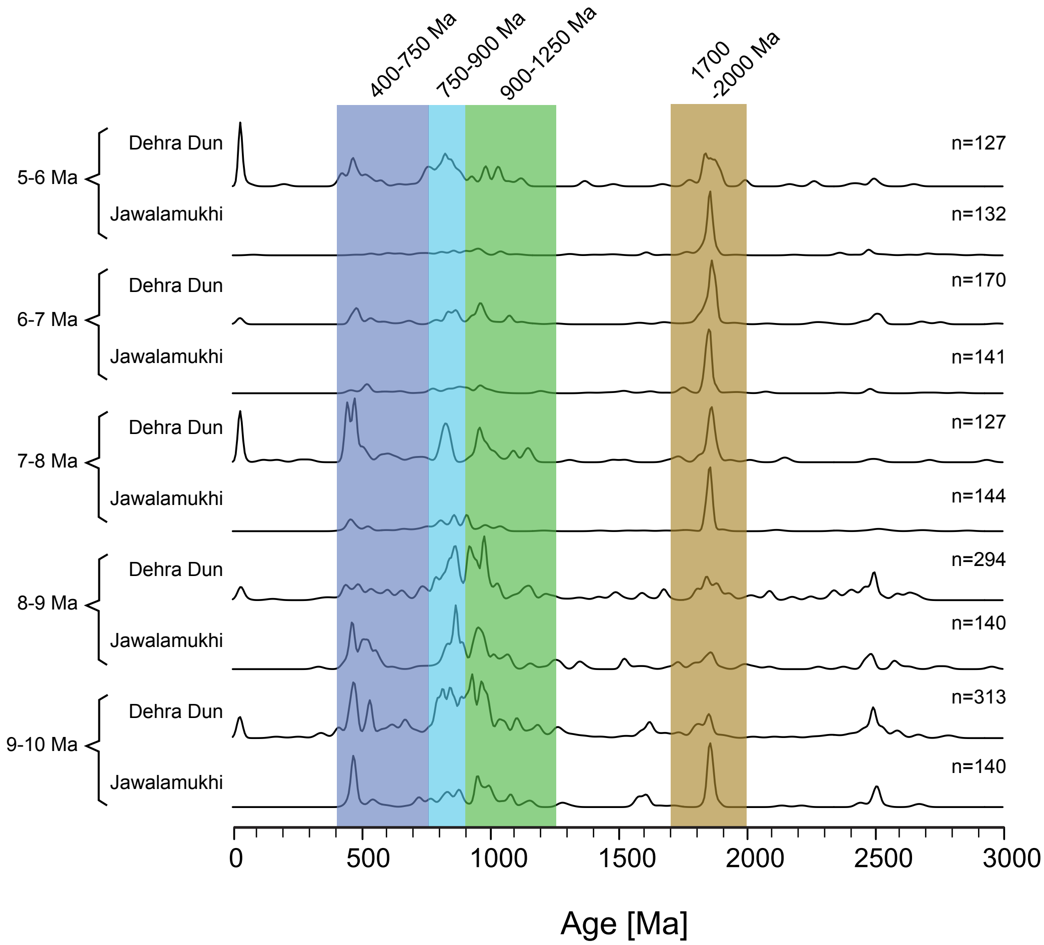

Figure 9
Exnicios et al.

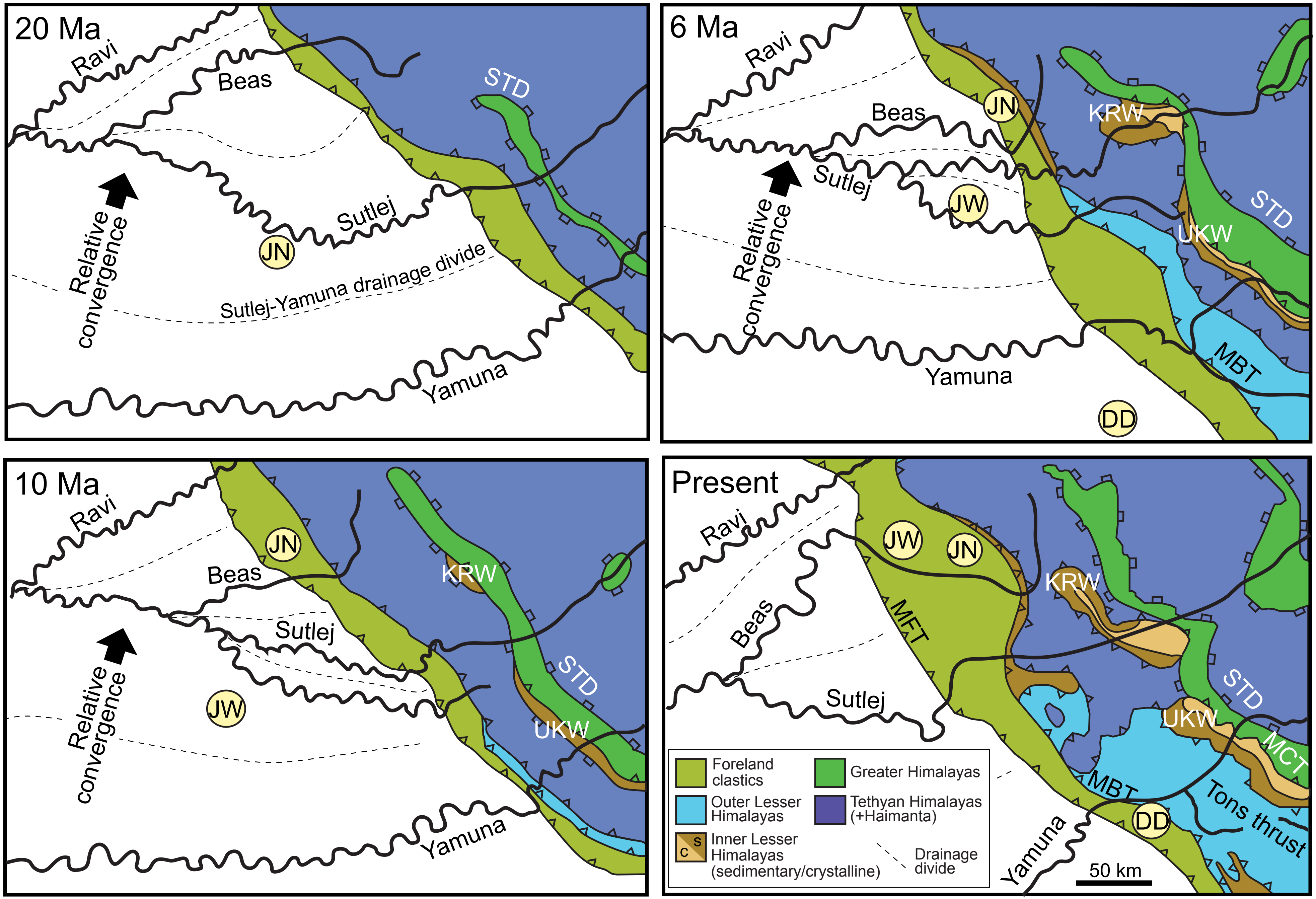

Figure 10
Exnicios et al.